Bulk Met and Fluxes

Version 1, Aug 2022, BWB

The first field research intensive of the Fog And Turbulence Interactions in the Marine Atmosphere (FATIMA) project occurred in July 2022, with two primary research platforms/sites in the Eastern North Atlantic near Nova Scotia and Newfoundland: a fixed station on Sable Island, and ship cruise on PSV *Atlantic Condor*. This report covers bulk meteorology and turbulent flux measurements on PSV Condor with the NOAA Physical Sciences Laboratory NOAA Air-Sea Flux System. The ship cruise track, from July 4 to August 1 is shown in Figure 1. Cruise leg 1 was conducted largely in the vicinity of 46°N, 48°W near the Hibernia offshore oil platform, followed by a brief resupply stop in St. John's, Newfoundland. Leg 2 focused on the area around Sable Island and concluded with a transect south to warmer waters in the Gulf Stream at 60.5°W, 39.5°N.

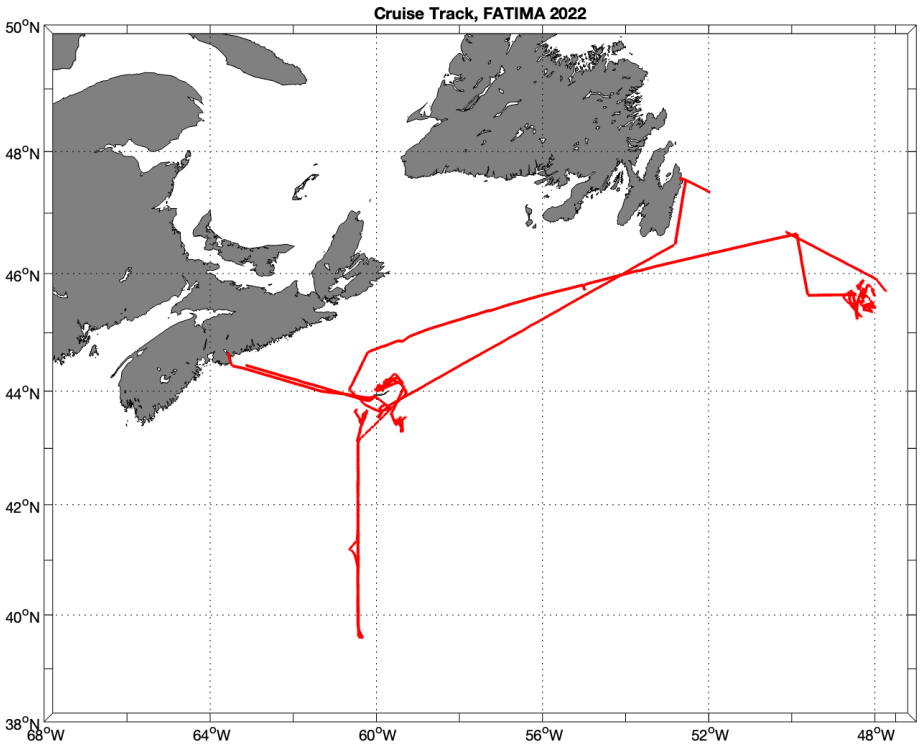

Figure 1: PSV Atlantic Condor cruise track. Gaps are periods of missing GPS data.

The NOAA Air-Sea Flux System consists of a set of sensors mounted at the top of the bow mast, a second set on the pilot house roof, and an ocean surface temperature sensor deployed from the starboard railing. Bow mast sensors include: one Gill R3A ultrasonic anemometer (@20 Hz), one LICOR 7500A fast water vapor infrared gas analyzer (@10 Hz), one Vaisala WXT520 weather transmitter (temperature, RH, pressure, rain and wind speed/direction @ 1Hz), and one Inertial Labs MRU-P motion sensor (@20 Hz).

The pilot house roof components include: one Hemisphere Crescent VS100 GPS heading system (@1 Hz), one Vaisala HMP pressure sensor, a pair of Eppley PIR pyrgeometers for downwelling IR flux, and Kipp & Zonen CM22 and CMP22 pyrometers for downwelling solar radiative flux. The sea surface temperature measurement was a YSI 46040 precision thermistor in a custom-fabricated hose (i.e. the NOAA 'sea snake'). The SST measurement is at approximately 5 cm depth. Data rates for all except heading are 1 min^{-1}, recorded with a Campbell Scientific CR-1000 data logger. Figures 2 and 3 show the bow mast installation and sea snake davit on the forward starboard railing, respectively.

Figure 2: Bow mast installation: Gill R3A center top, LICOR 7500 on left, and Vaisala WXT on right. The IMU and GPS antenna are below the Gill R3. Height for the Gill R3A is 18.6 m ASL.

Figure 3: Sea snake position on the forward starboard-side railing. SST is recorded at 1 min^{-1} by a Campbell Scientific CR-1000 data logger located on the pilot house roof.

All data streams are serial strings, saved to hourly files on a Windows PC located in a container lab on the main deck.

This document provides an overview for Version 1 of the bulk meteorological and turbulent flux measurements. Final results are presented at 10-min and hourly timescales. The 10-min results are crudely filtered to remove periods of known instrument malfunction and outliers. The hourly file is produced from the 10-min output, with more selective filtering for turbulent flux parameters. Filtering criteria are described in Appendix 1.

The complete dataset includes raw hourly files, processed intermediate results at at various timescales (1 Hz, 1-min and 10-min), final results at 10-min and hourly timescales, diagnostic and analysis plots, and Matlab/python code for all data analysis procedures. A full description of files and directory structure is given in Appendix 2.

Navigation / motion

In this analysis, data from the Hemisphere GPS heading system and Inertial Labs IMU provide the basis for true wind calculations and motion corrections to high-rate wind measurements. Standard deviations in ship speed-over-ground (SOG) and heading are shown in Figures 4 and 5. The IMU provides a second set of heading and GPS data. These are provided as raw files, but not used in this analysis. The IMU also provides derived pitch/roll angles and 3-axis velocities, in addition to raw 3-axis accelerations and rotational rates. In this version of the flux dataset we perform wind motion corrections in the usual way, from the accelerations and rotational rates (Edson et al., 1998) and do not use angles and velocities provided by the IMU. We may revisit this in a future release.

In addition to motion corrections, GPS and IMU statistics are used to filter 10-min turbulence parameters. In this analysis we impose limits on 10-min standard deviations of heading, SOG, and platform port-starboard velocity (from ship roll). See Appendix 1 for details. An additional limit on SOG is typically applied, but here we set it above the maximum ship speed and accept measurements from any period when SOG is relatively constant (i.e., the SOG standard deviation is below the specified limit).

Note, navigation data is not available from the ship systems for this cruise and there are no meteorological or oceanographic measurements from ship systems.

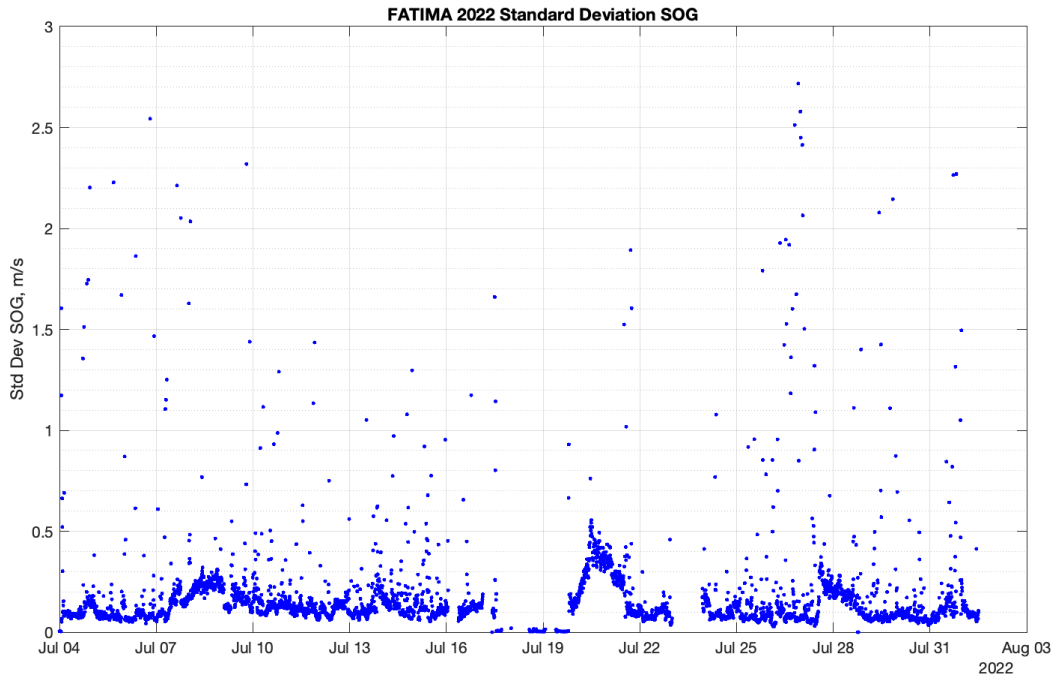

Figure 4: Standard deviation (10-min) in ship speed-over-ground.

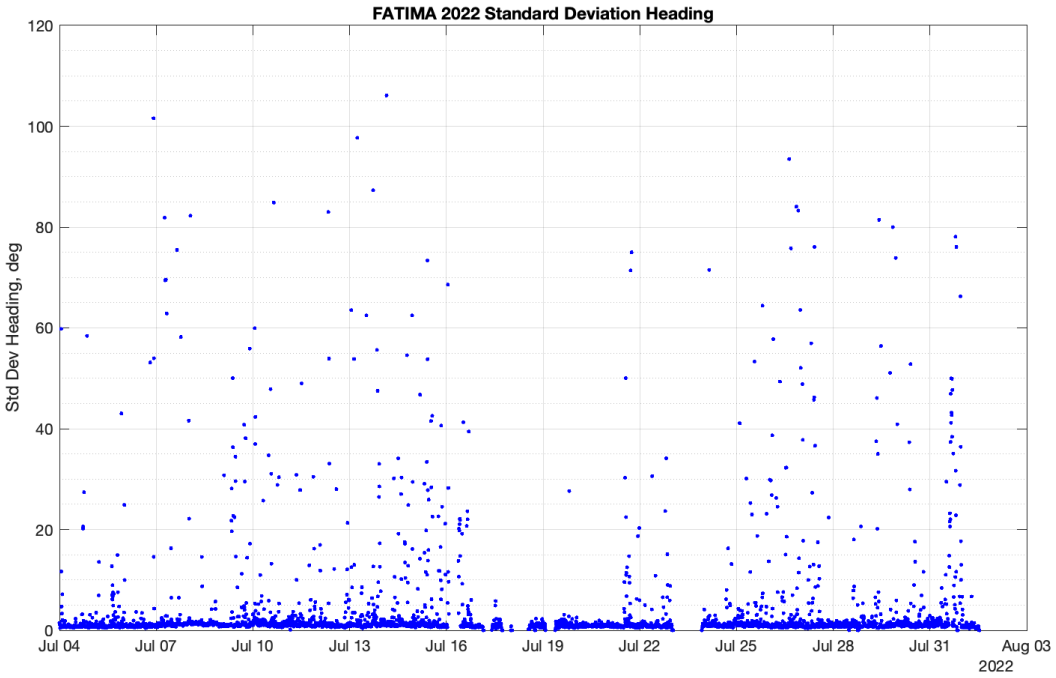

Figure 5: Standard deviation (10-min) in ship heading.

Wind

Primary wind velocity measurements are from the Gill R3A ultrasonic anemometer. Secondary wind data are available at 1 Hz from the WXT weather station. In most cases the two measurements compare very well, but the WXT sensor is blocked by the sonic mount at relative wind directions of ~ –90°.

True wind speed and direction are computed from the R3A 3-axis winds after tilt rotation and correction for ship speed and heading, including an approximate correction for flow distortion effects of the ship superstructure; the bow-stern (U) component of the wind is increased by 5% and the port-starboard (V) component reduced by 15%. This correction is appropriate for measurements at ~ 18m height on the bow mast of most global class research vessels. There are no comparison data for evaluating specific flow distortion effects on PSV Condor, so we assume the general correction is applicable here.

Figures 6-8 show true wind speed and direction from the R3A and WXT sensors. Wind direction during the cruise was predominantly from the SW. Figures 9-10 show the relative wind direction and distribution with respect to the ship's bow.

The mean ~ 6° streamline tilt angle for FATIMA (Figure 11) is similar other ships (e.g. RV Brown, RV Thompson, RV Knorr). Tilt is relatively constant over a wide range of relative wind direction, which is unusual. The standard deviation in vertical wind was also mostly constant over a wide sector (see following section on turbulence measurements). Therefore, in this analysis we apply a relatively wide relative wind direction sector of +/- 90° for 'good' turbulence data.

True wind speed and direction is crudely filtered to a relative wind direction sector of +/- 120°. There are no secondary sources of wind data from the stern, so this data set does not include wind data for relative directions outside this sector.

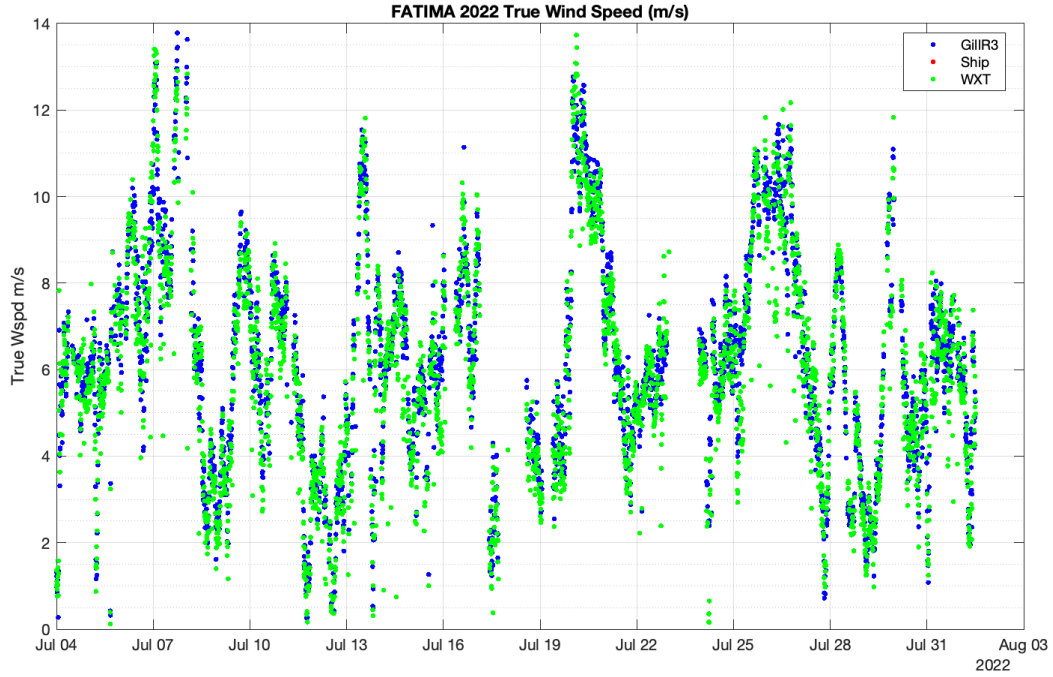

Figure 6: True wind speed

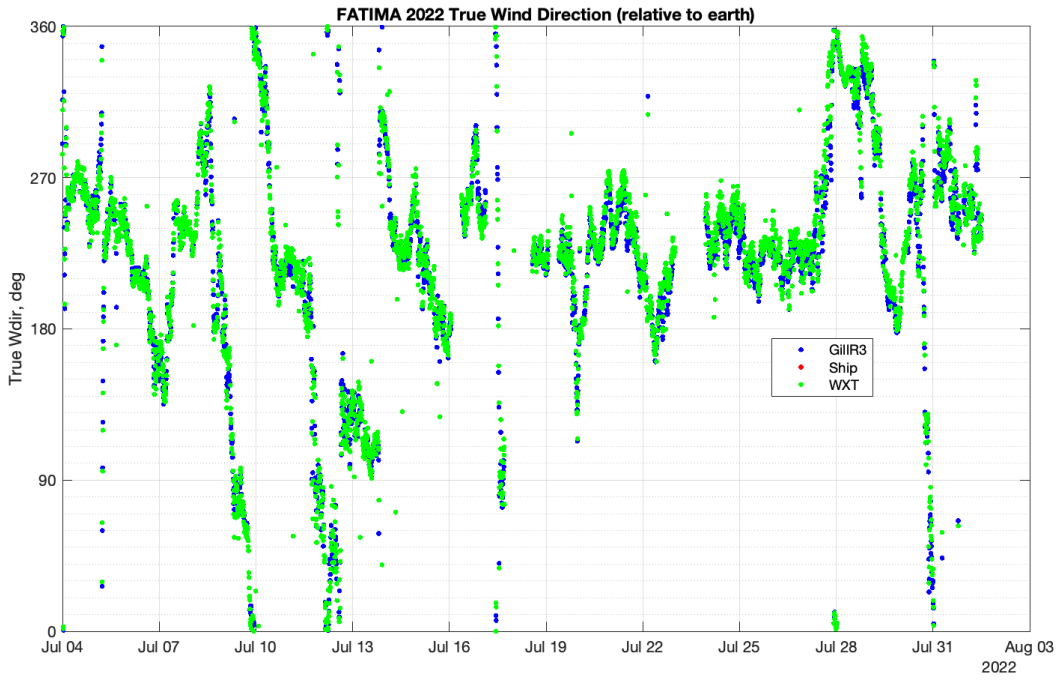

Figure 7: True wind direction

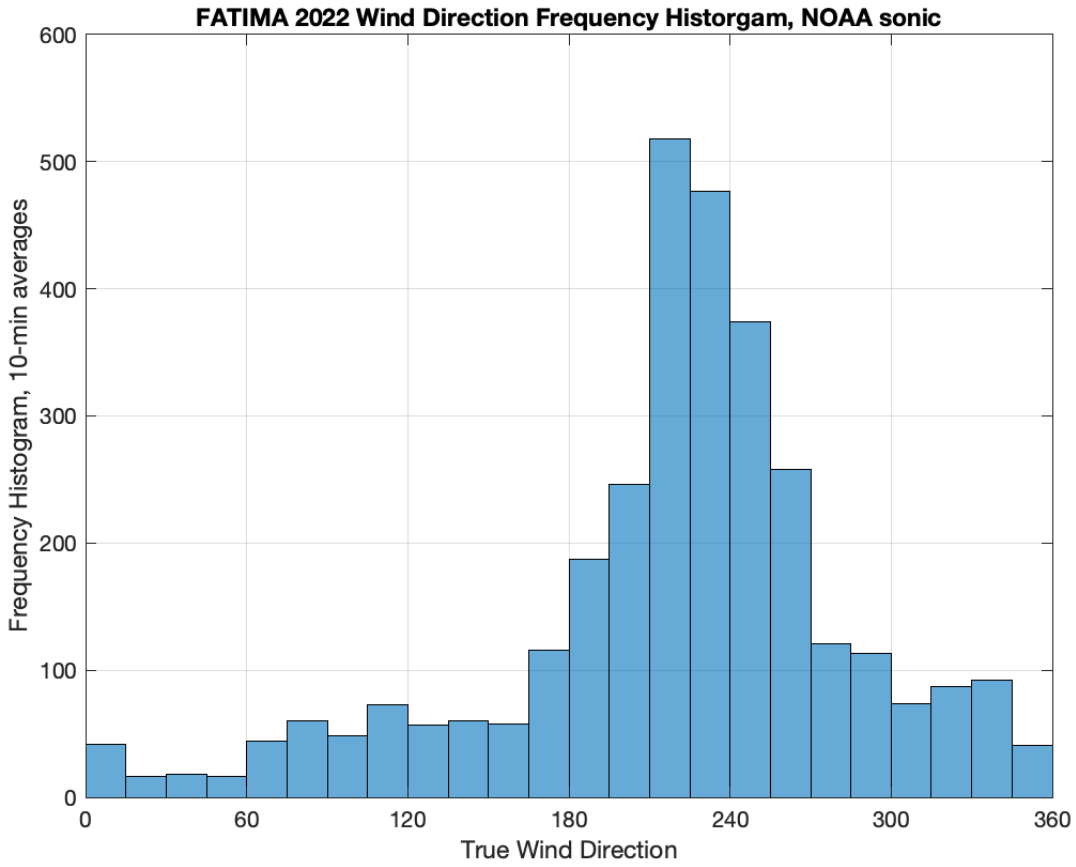

Figure 8: Distribution in 10-minute true wind direction. Southwesterly winds for most of the cruise.

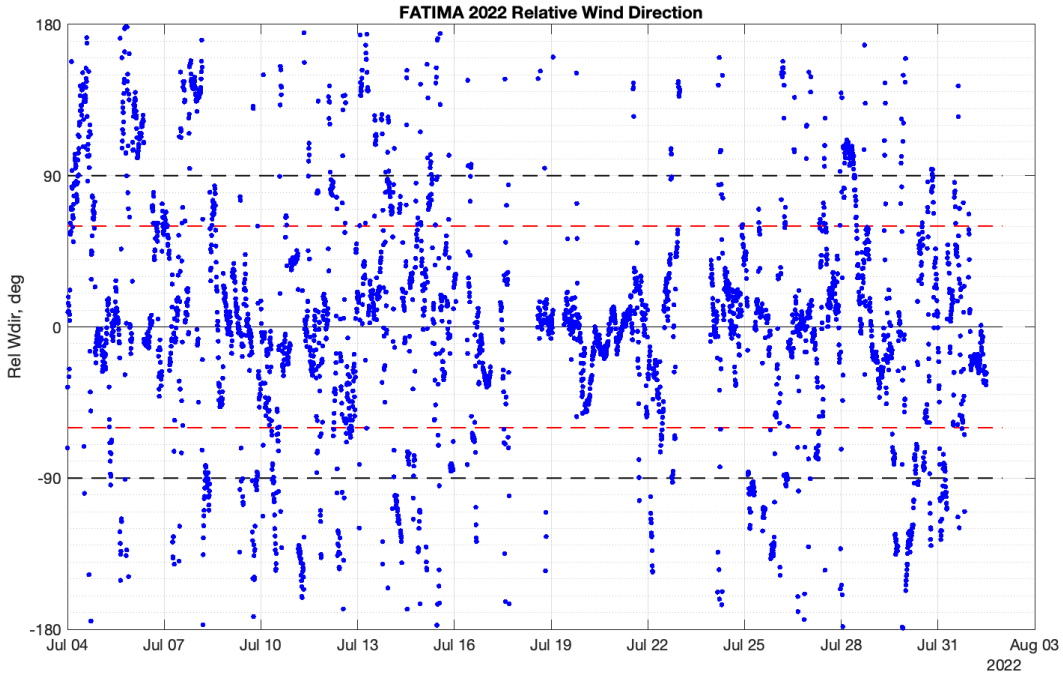

Figure 9: Relative wind direction, with respect to the ship's bow.

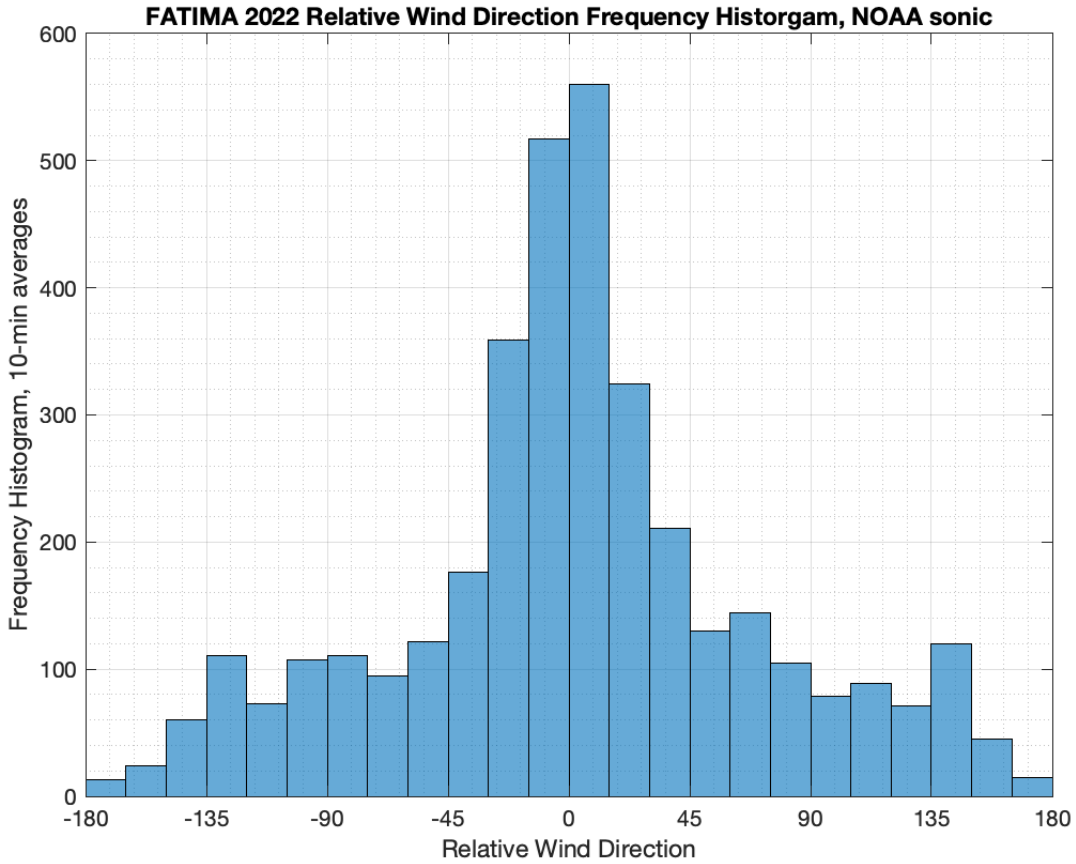

Figure 10: Distribution of 10-min relative wind direction.

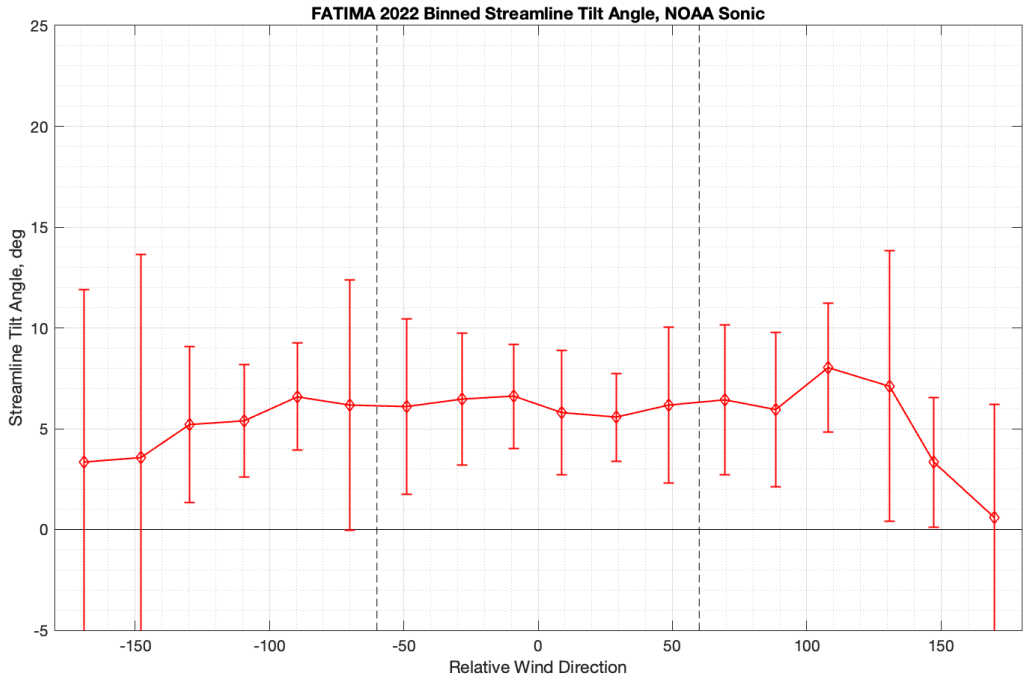

Figure 11: Wind streamline tilt angle at the top of the bow mast.

Air temperature, RH, pressure

Figures 12-14 show air temperature, relative humidity and sea level atmospheric pressure for the entire cruise. The bow tower WXT is the primary measurement for temperature and RH. The Vaisala PTB is the primary pressure measurement, but duplicate pressure measurements from the WXT are almost identical.

Case and dome temperatures from the two Eppley pyrgeometers are a secondary air temperature reference. Nighttime PIR temperatures equilibrate to the mean air temperature. These are recorded at lower resolution (~ 0.2°C) but the four PIR sensors are virtually identical in magnitude at night. Analysis of nighttime temperatures from Leg 1 show a bias of –0.51°C in the WXT air temperature relative to the mean PIR sensors (Figure 15). This might suggest an adjustment of air temperature is necessary. However, bulk comparisons for heat fluxes are all much better if we do not make an air temperature adjustment. The reason for the offset requires further investigation, so we have not made an adjustment to air temperature in this version of the met/flux dataset.

Sea surface temperature

Two SST measurements are available for FATIMA: the NOAA sea snake at ~ 5 cm depth and the Notre Dame Remote Ocean Surface Radiometer (ROSR) surface skin temperature (Figure 16). There are no ship SST data. The sea snake operated reliably until July 17 0600 UTC. After this time sea snake data were corrupted, most likely due to salt and moisture in a cable connection.

During the period when both SST systems were valid, agreement between the sea snake and ROSR is quite good, with a mean bias of -0.2°C between the ROSR and sea snake (Figure 16). This is approximately the correct magnitude for cool skin temperature depression.

In this analysis, 10-min mean ROSR SST is the primary reference for computing bulk fluxes. Because the ROSR is surface skin temperature, the COARE bulk model cool-skin option is not used.

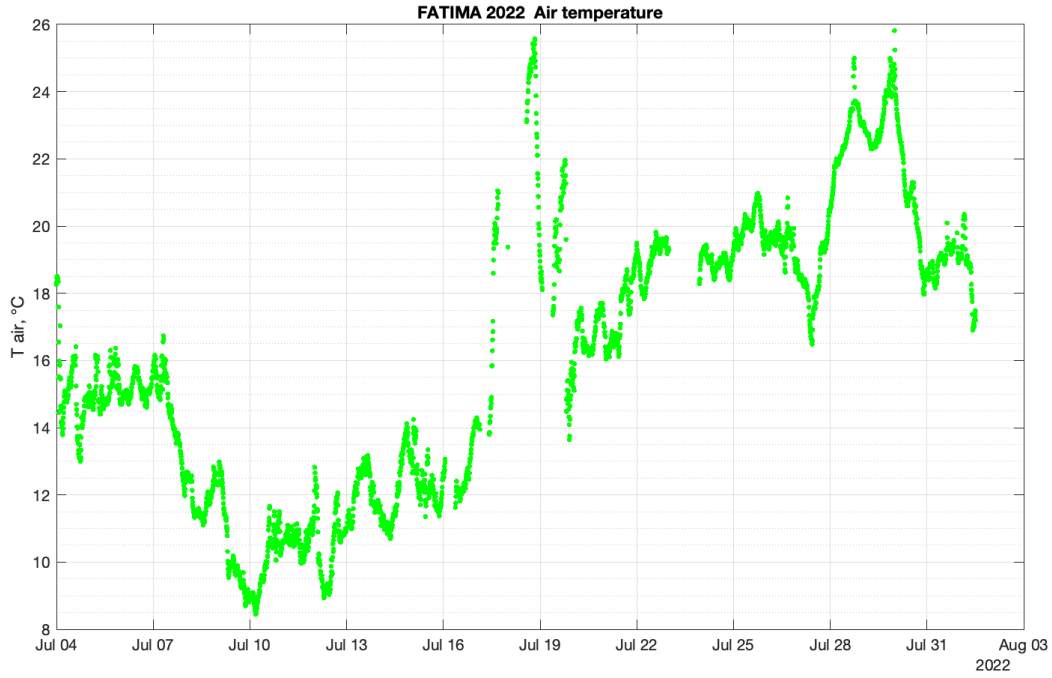

Figure 12: Air temperature, bow tower WXT.

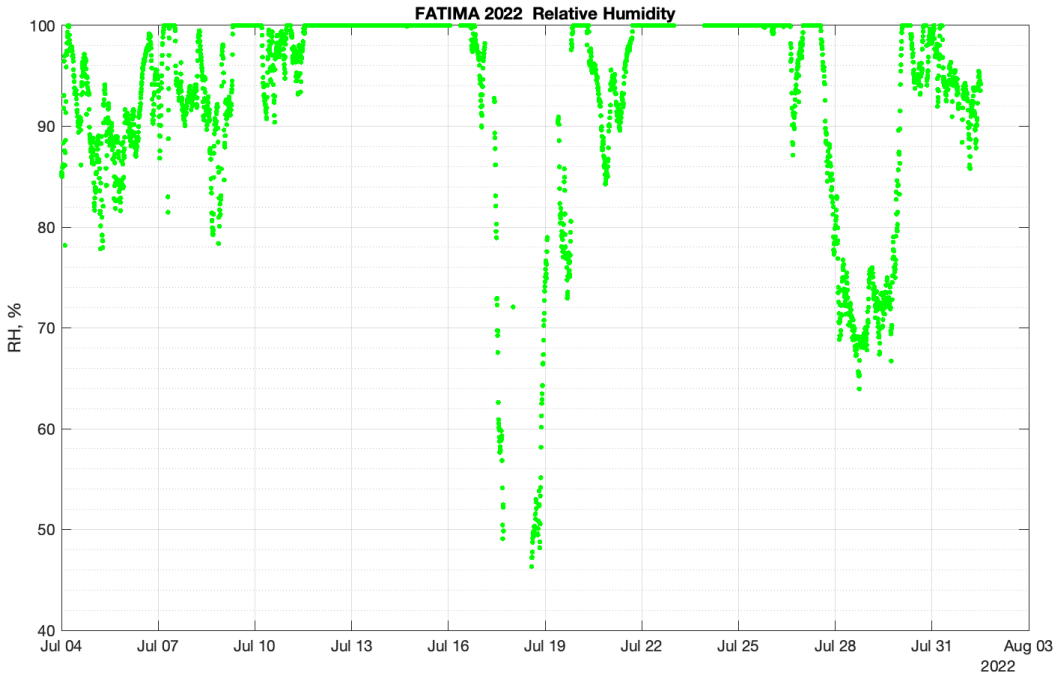

Figure 13: Relative humidity, bow tower WXT.

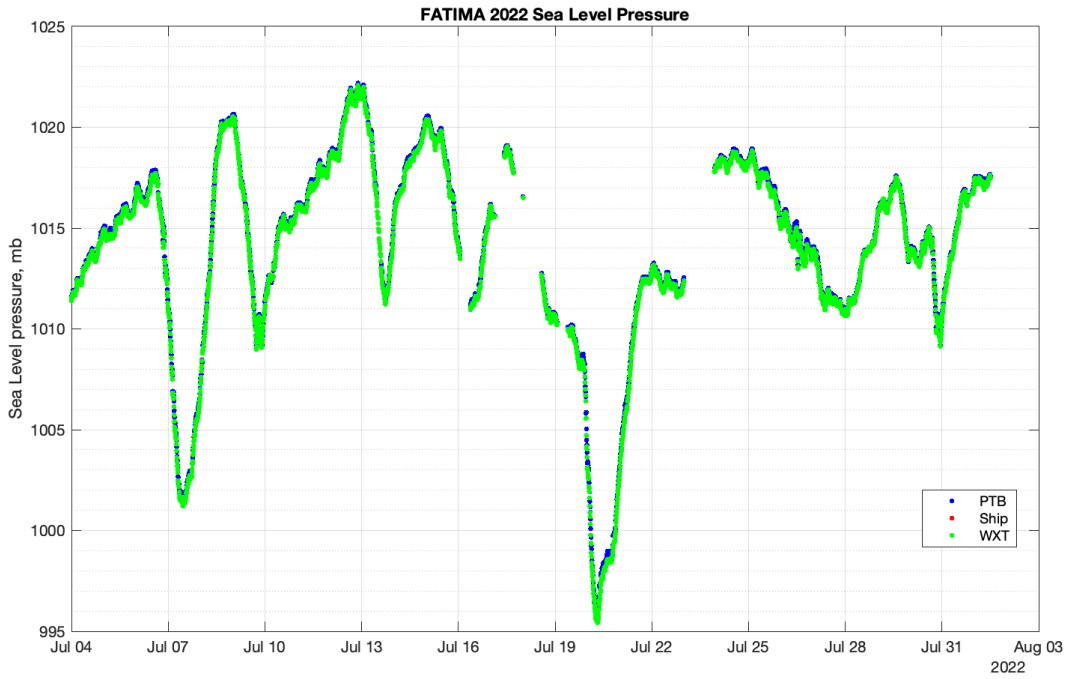

Figure 14: Sea level adjusted atmospheric pressure, bow tower WXT and Vaisala PTB.

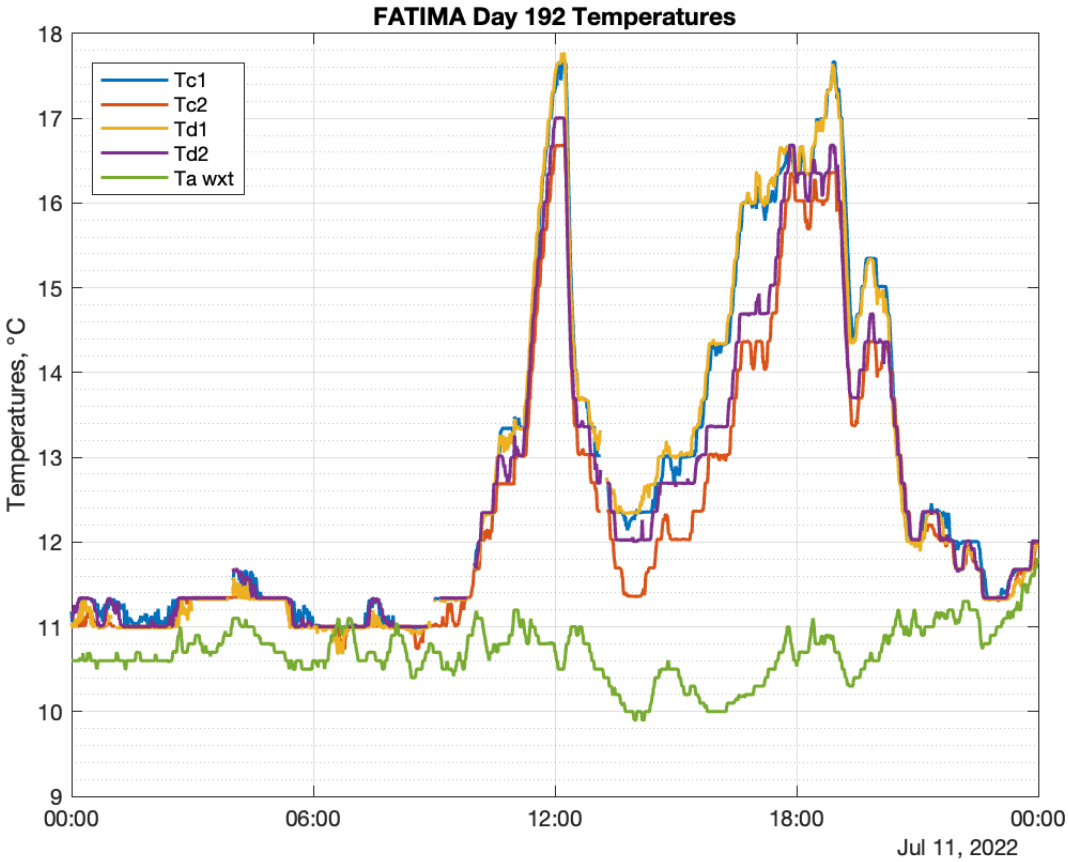

Figure 15: WXT air temperature and PIR case/dome temperatures on July 11. Night time hours are ~ 23:00 to 09:00 UTC.

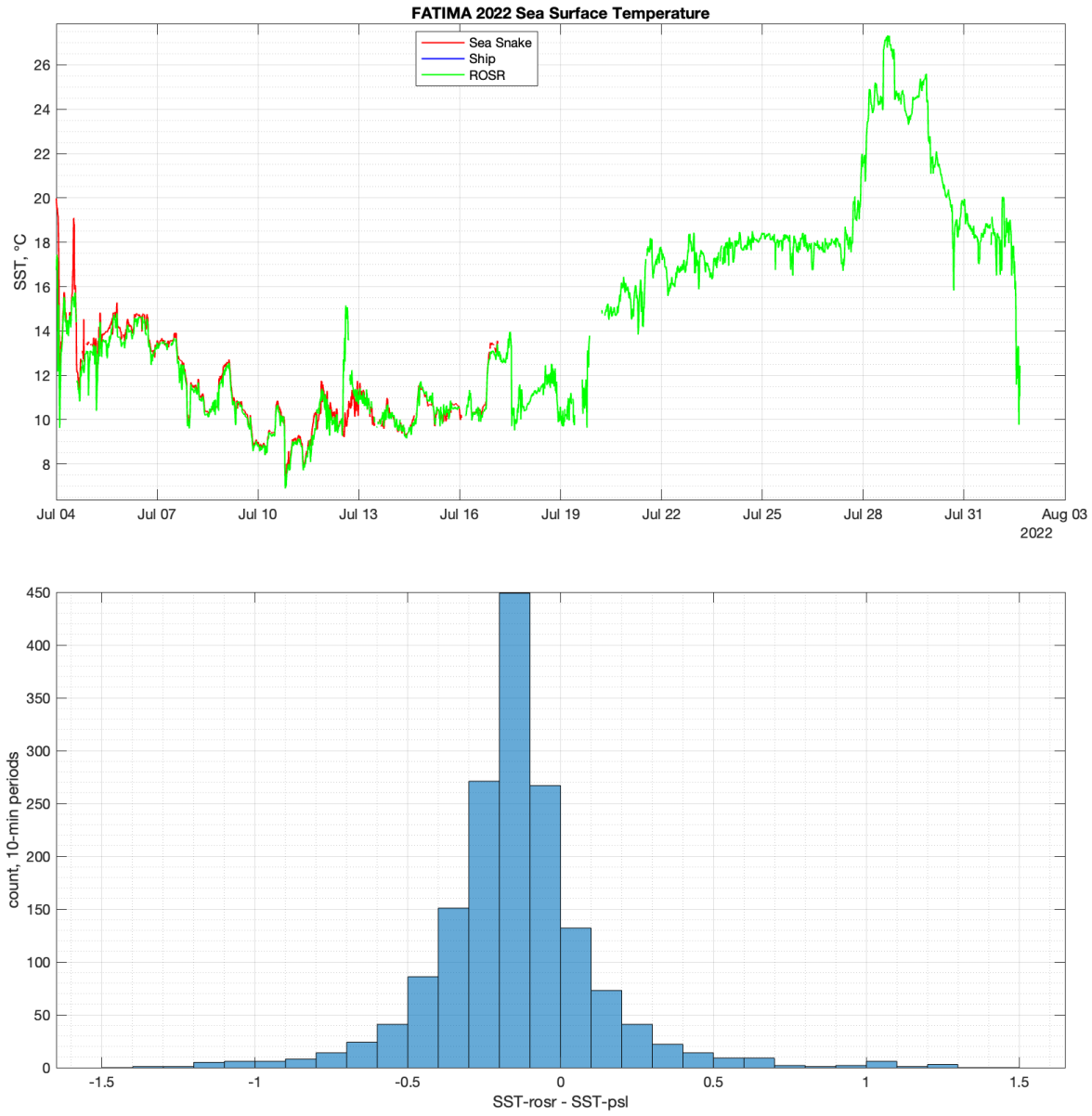

Figure 16: Sea surface temperatures from the NOAA 'sea snake' and Notre Dame ROSR. The mean difference indicates a cool skin temperature depression of ~ – 0.2°C.

Solar and infrared radiation

Duplicate solar and IR radiometers were deployed for this cruise. In this analysis the mean for each pair is used for downwelling solar and IR flux. Solar downwelling flux closely approximates the expected clear sky value (M. Iqbal, 1988) on clear days during the cruise (July 5 and July 27-29, Figure 17). Most other days show decreased solar flux from combined effects of low clouds and fog. Downwelling IR flux (Figure 18) is also very close to the expected clear sky values on July 5 and 28. On overcast days, downwelling IR flux is enhanced by warm, low-level clouds and fog.

Daily mean cloud forcing terms are shown in Figure 19 and the daily mean net heat budget is in Figure 20, computed from downwelling solar and IR radiation (R_{solar} , R_{IR}) with bulk model estimates for sensible, latent, and rain heat fluxes, where

$$H_{net} = 0.955\, R_{solar} - R_{netIR} - HS - HL - H_{rain}$$

$$R_{netIR} = 0.97(5.67 \times 10^{-8}\, SST(K)) - R_{IR}$$

On a daily basis, there is net warming to the ocean of 80-300 W/m^2. To compute daily means, gaps of up to 3 hours were filled by interpolation and means are reported only for days with 24 hours of data.

Hourly heat budget components are shown in Figure 21. The net is negative during clear-sky nights on July 4-5 and July 28-29. The latent heat contribution is near zero or positive during high-humidity, foggy conditions and strongly negative during the Leg 2 south transect into the Gulf Stream. Sensible heat flux contributions are positive and fairly small in the colder water near Hibernia platform and Sable Island, and slightly negative during the south transect.

Rain rate

The WXT acoustic rain sensor is used in this analysis for a bulk estimate of rain heat flux. Rain observations can be highly variable and careful comparison with the Notre Dame Meter Microwave Rain Radar (MRR) is a good idea. However, rain is typically a small contribution to the net heat flux.

Rain rate results are shown in Figure 22. Significant rain events were observed on July 7, 16, 18-20, and 29-30.

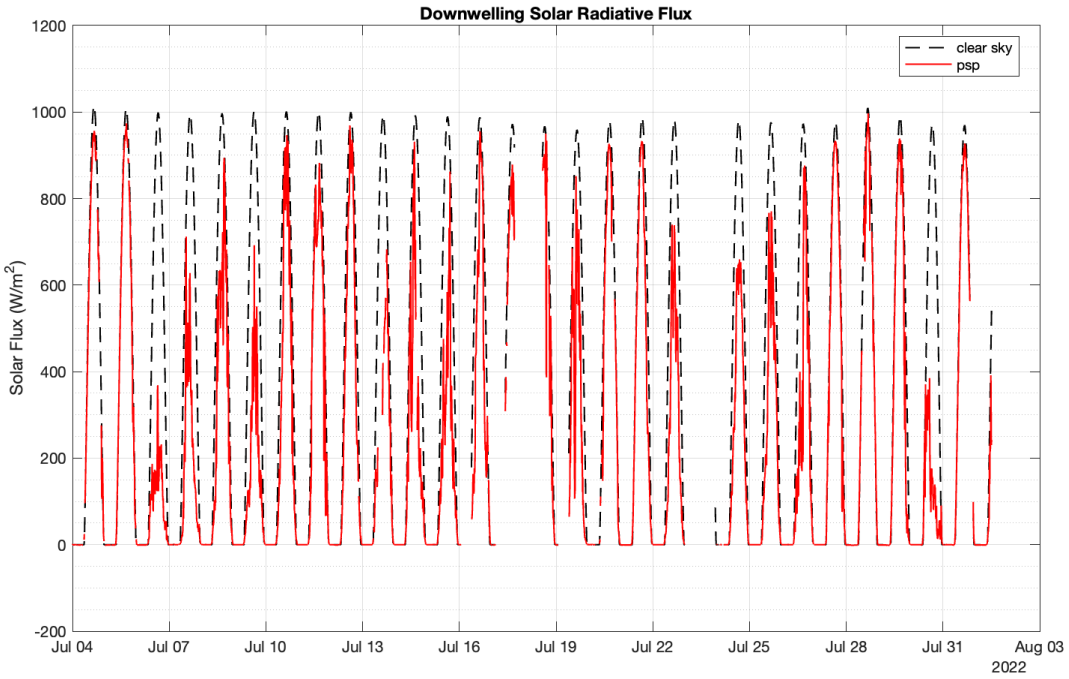

Figure 17: Solar downwelling radiative flux from the mean of CM20 and CMP20 measurements.

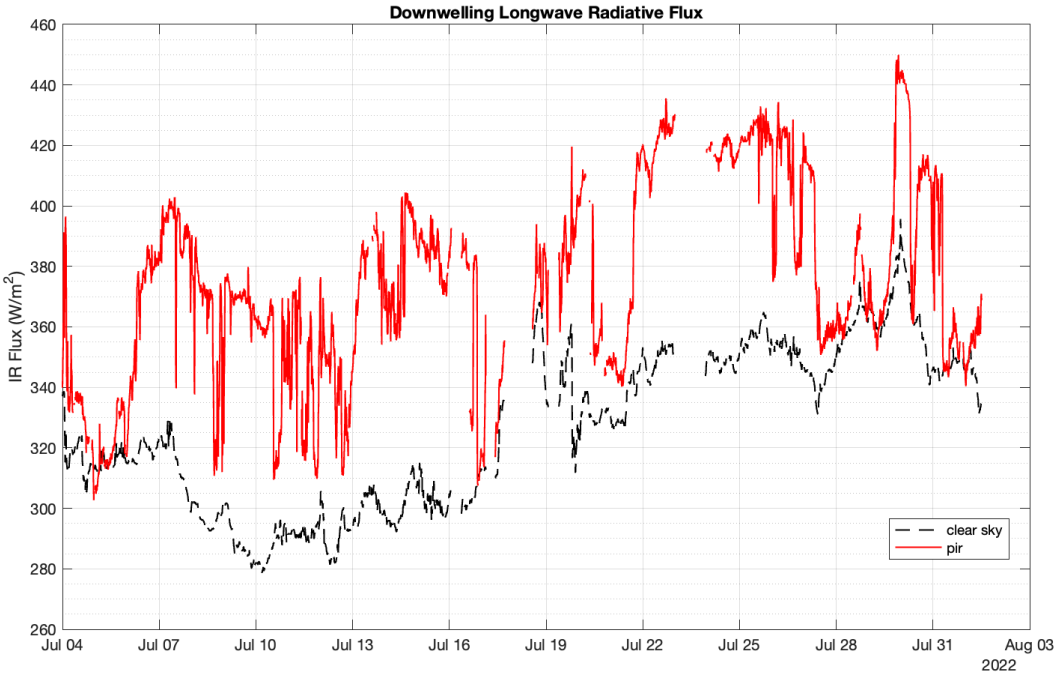

Figure 18: IR downwelling radiative flux from the mean of PIR1 and PIR2 measurements.

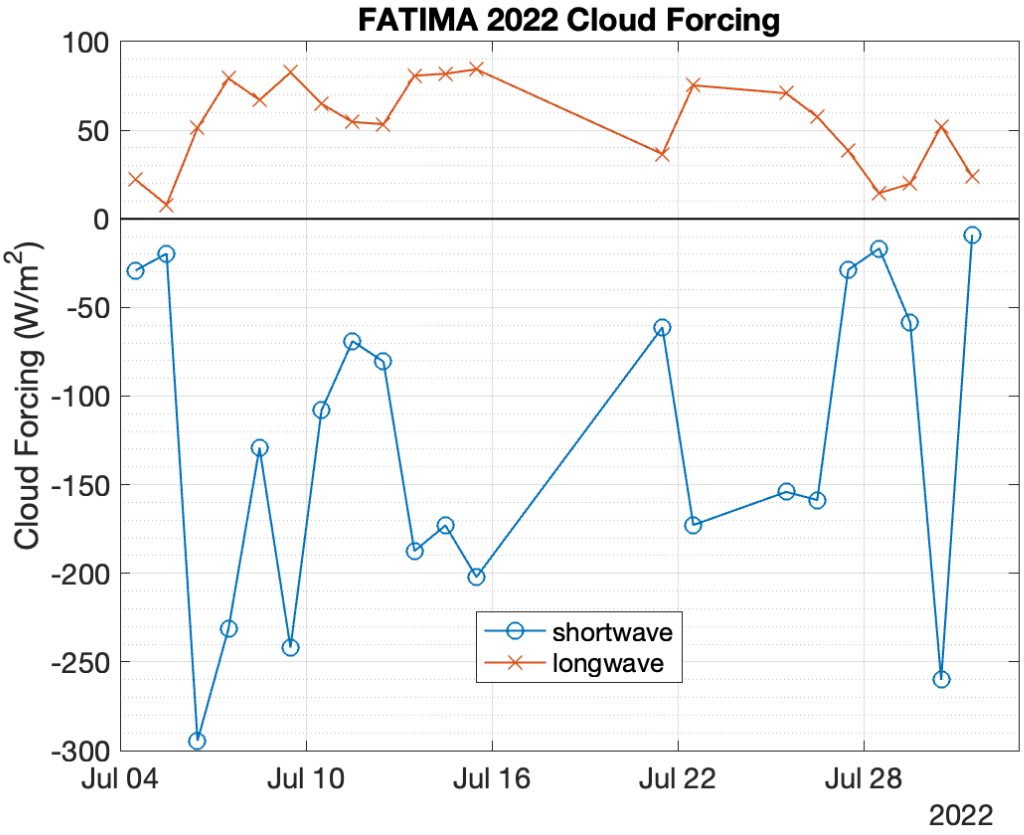

Figure 19: Daily mean solar and IR cloud forcing with respect to clear sky conditions.

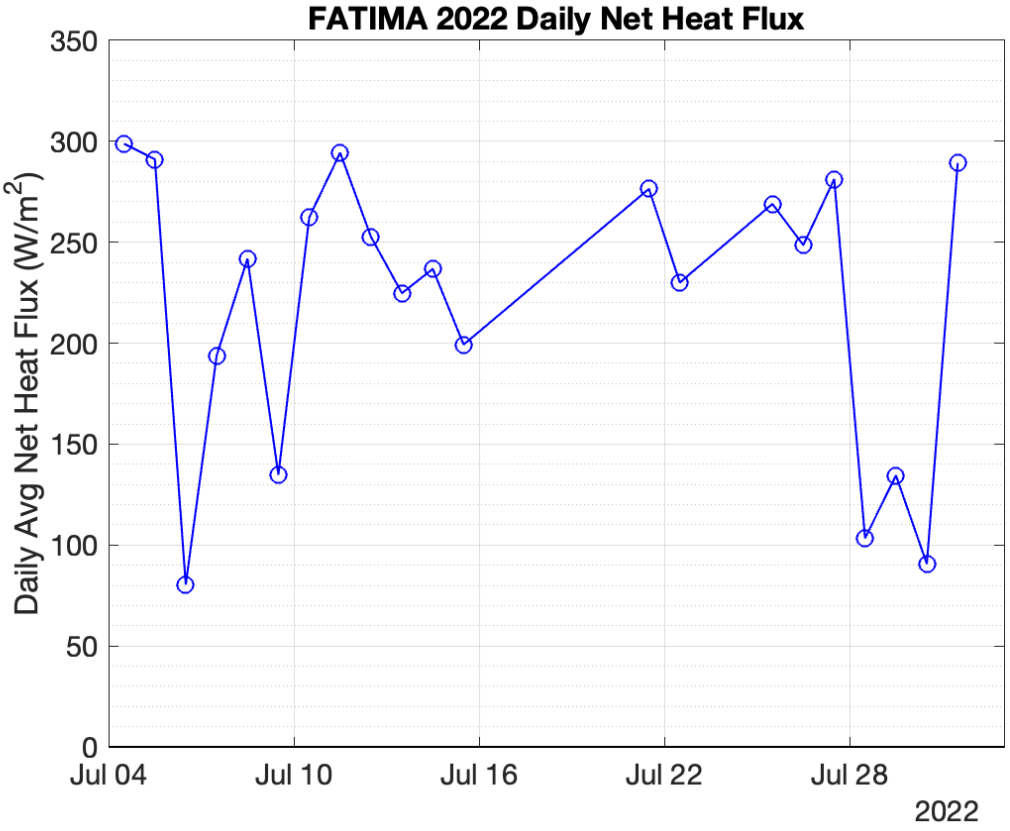

Figure 20: Daily mean net heat flux.

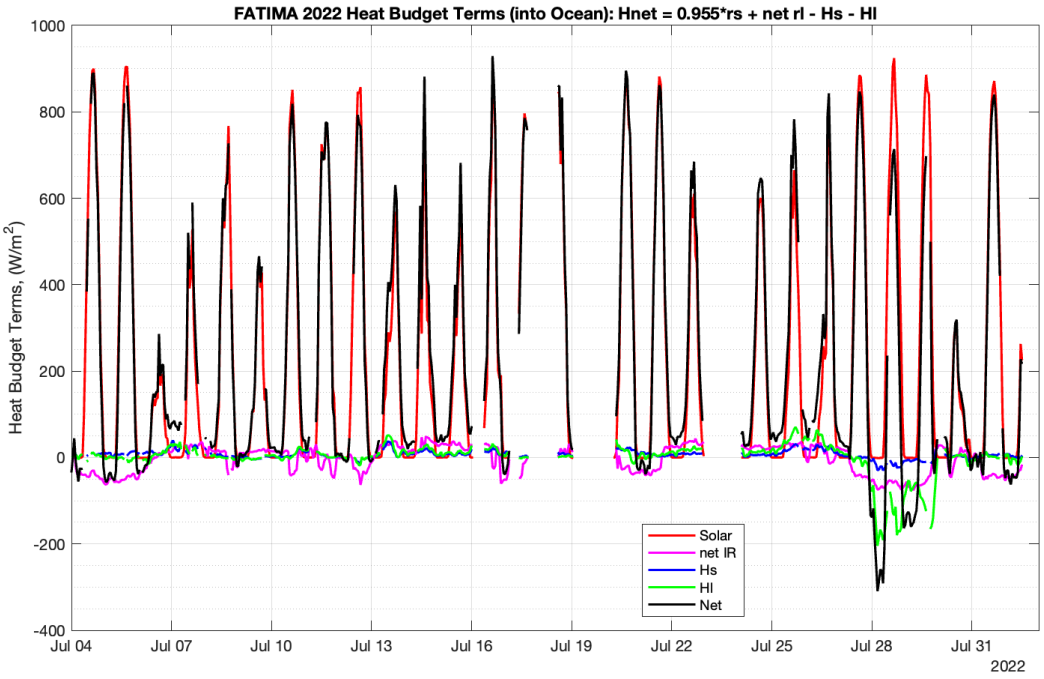

Figure 21: Hourly net heat budget terms with respect to the ocean. Sensible and latent heat fluxes are bulk model values.

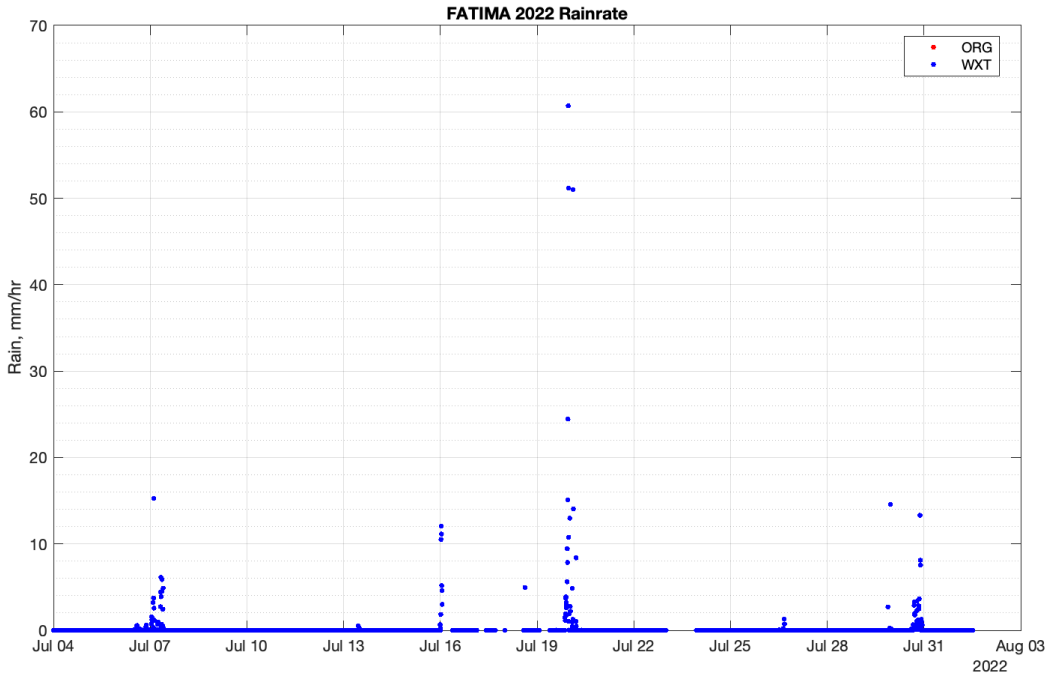

Figure 22: Rain rate from the bow tower WXT.

Turbulence variables and fluxes

Raw sonic anemometer data were affected by noise spikes and interference from an unknown source. The sonic for Leg 1 was replaced with the spare Gill R3A during the mid-cruise layover in St John's. Interference issues were reduced in Leg 2, but not entirely absent. Interference with sonic temperature measurements was especially severe, with large positive and negative spikes at irregular intervals and decay times of several minutes. Spikes in wind data were usually coincident with the temperature spikes, but limited to a single data point. Figure 23 shows a hour of raw sonic data from July 12.

For this analysis, spikes larger than 2.5 standard deviations from the detrended 10-min mean are removed from wind and sonic temperature data and replaced with interpolated values. For flux calculations, 10-min sonic temperature variance is limited to 0.15°C. Temperature data with large spikes, as shown in Figure 23, are mostly unusable. In general, single-point random noise spikes are uncorrelated with vertical wind or scalar fluctuations, and should not bias the flux measurement, but will increase measurement uncertainty.

From the MOST relationship for vertical wind standard deviation (after Kaimal and Finnigan, Eq. 1.28 & 1.33, p.16)

$$\sigma_w = 1.25\, u_* \Psi(z/L)$$

we expect the quantity $\sigma_w/(u_* \Psi(z/L))$ to have a constant value of ~ 1.25. Figure 24 shows the observed value during FATIMA is greater than 2.0. This is unusual based on our experience from prior cruise projects, implying residual noise in the wind velocity measurement. However, this result is roughly constant over a very broad wind sector, similar to the tilt angle result in Figure 11. This supports a relative wind direction sector of at least +/- 90° for acceptable conditions of limited flow distortion.

The normalized standard deviation of vertical velocity (W) is mostly consistent with the expected MOST relationship (Figure 25) but also indicates excessive vertical wind variance in weakly stable conditions.

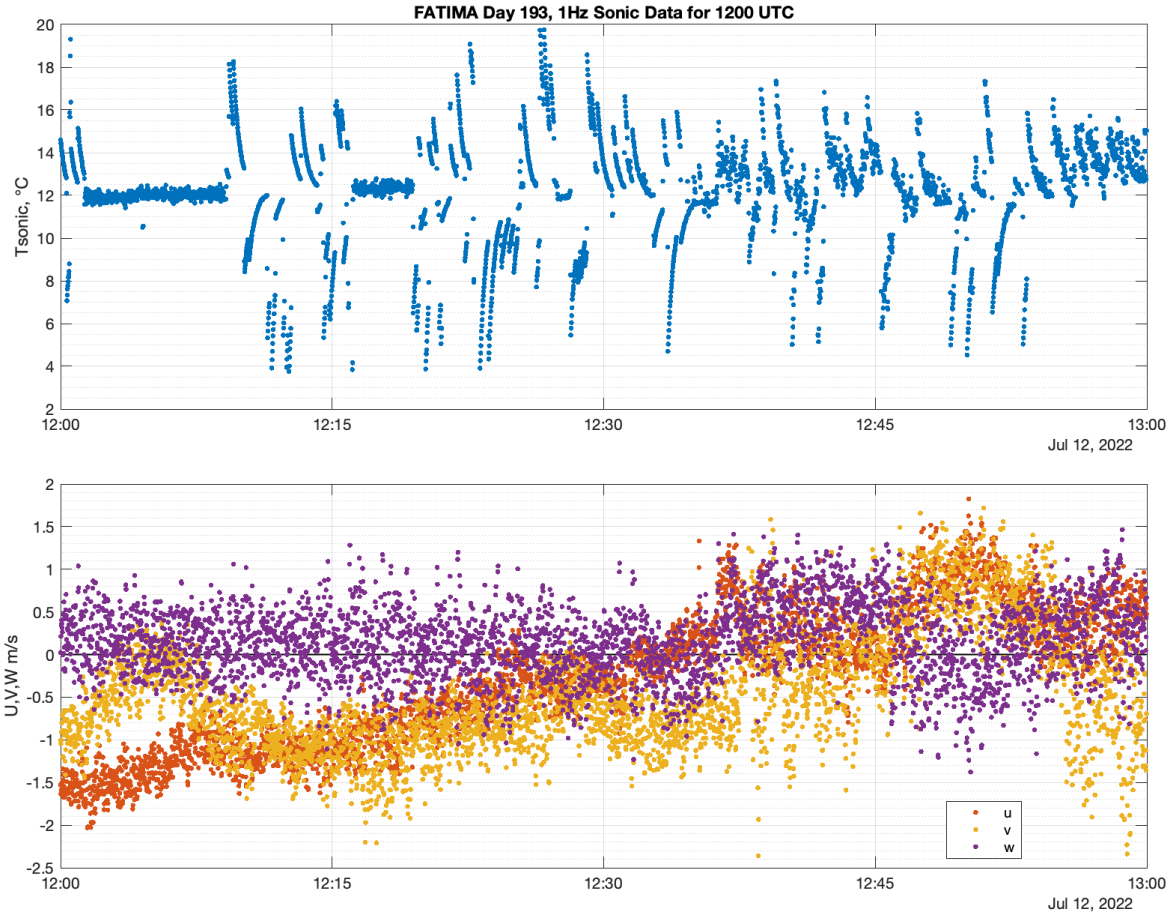

Figure 23: Raw sonic anemometer data for 1200 UTC, July 12, showing large spikes in sonic temperature data. Coincident spikes in UVW winds were less severe.

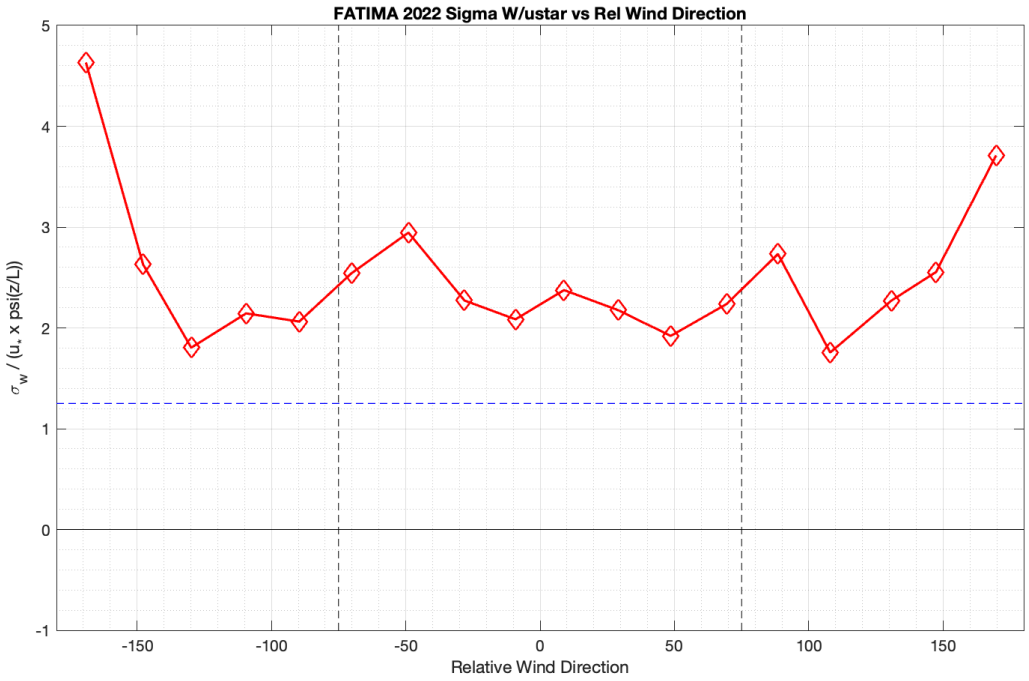

Figure 24: Normalized standard deviation in vertical velocity vs. relative wind direction.

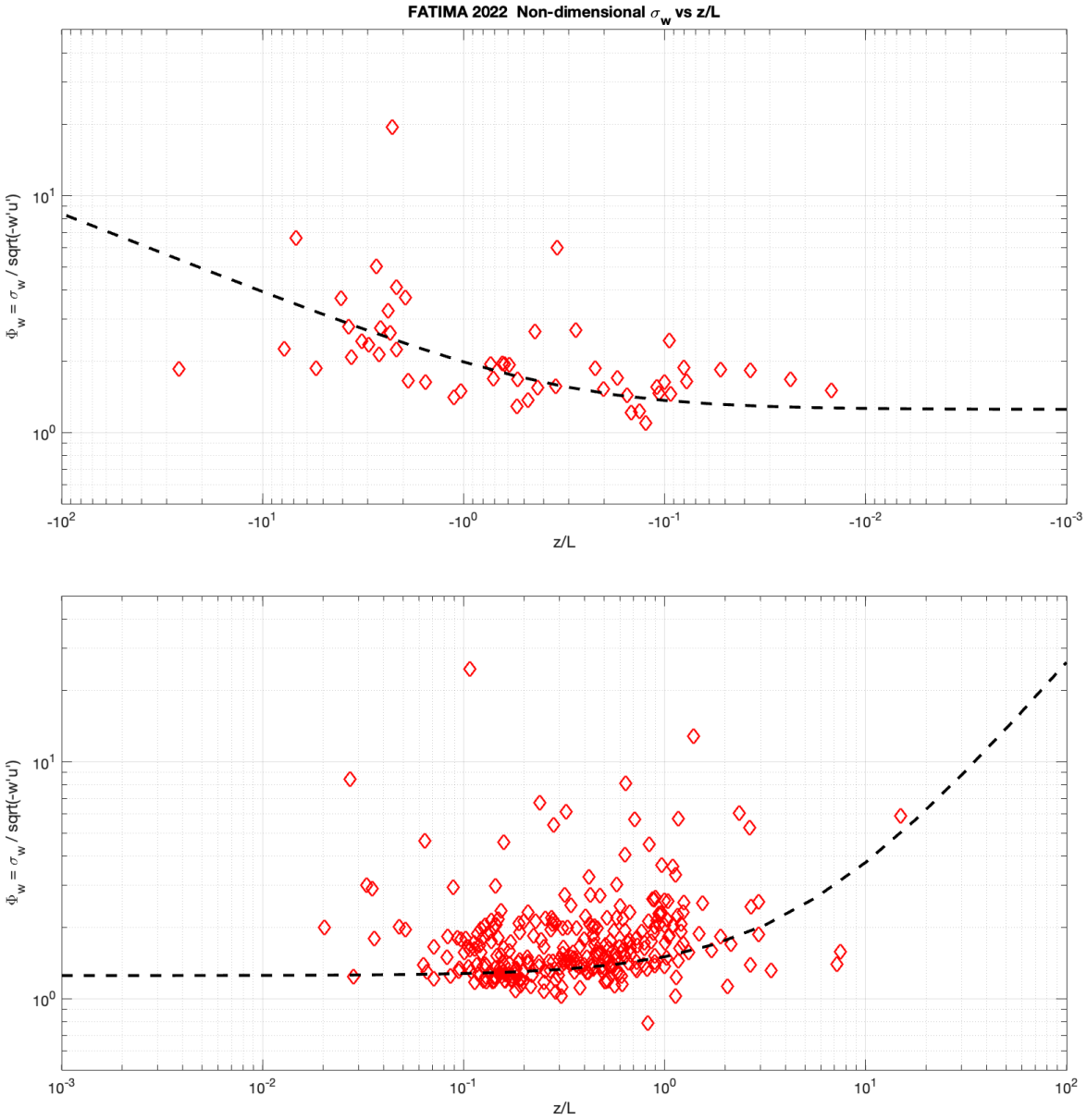

Figure 25: Normalized standard deviation in vertical velocity vs. z/L. Dashed line is the MOST relationship $1.25\,\Psi(z/L)$.

Stress and friction velocity

Turbulent stress and friction velocity was computed from the integral of the $w'u'$ cospectrum (with applied hamming window) and from the u and w spectra by inertial dissipation. For the cospectral (covariance) result, friction velocity is computed as

$$u_* = -\,sign(\overline{w'u'})\sqrt{|\overline{w'u'}|}$$

to preserve noise characteristics in the measurement at low wind speeds. A plot of covariance vs. bulk friction velocity (Figure 26) shows quite a few instances of negative u_*, however, which indicates spikes in the w'u' cospectrum rather than just random noise, yielding a positive result for the integral at moderately low wind speeds.

The inertial dissipation result (Figure 27) is less noisy and in good agreement with the bulk estimate from COARE 3.5. The filtered hourly time series for both covariance and ID results are shown in Figures 28 an d 29. The wind speed dependence of streamwise and cross-stream stress is illustrated in Figures 30 and 31.

Sensible heat flux

Covariance sensible heat fluxes are computed from the cospectral integral of $w'Tsonic'$ and by inertial dissipation from the respective spectra. Sonic temperature flux is adjusted for water vapor flux with u_* and q_* from the bulk model run

$$w'T' = w'Tsonic' - 0.51\,T_{air}(K)\,(-u_*\,q_*)$$

and the sensible heat flux is

$$HS = w'T'\,C_p\,\rho_a$$

where C_p is heat capacity and ρ_a is air density.

Time series of hourly filtered turbulent sensible heat fluxes by both methods are shown in Figures 32 and 33. As shown in Figures 34 and 35, both methods compare well with the COARE bulk value despite noise and interference with the Tsonic measurement.

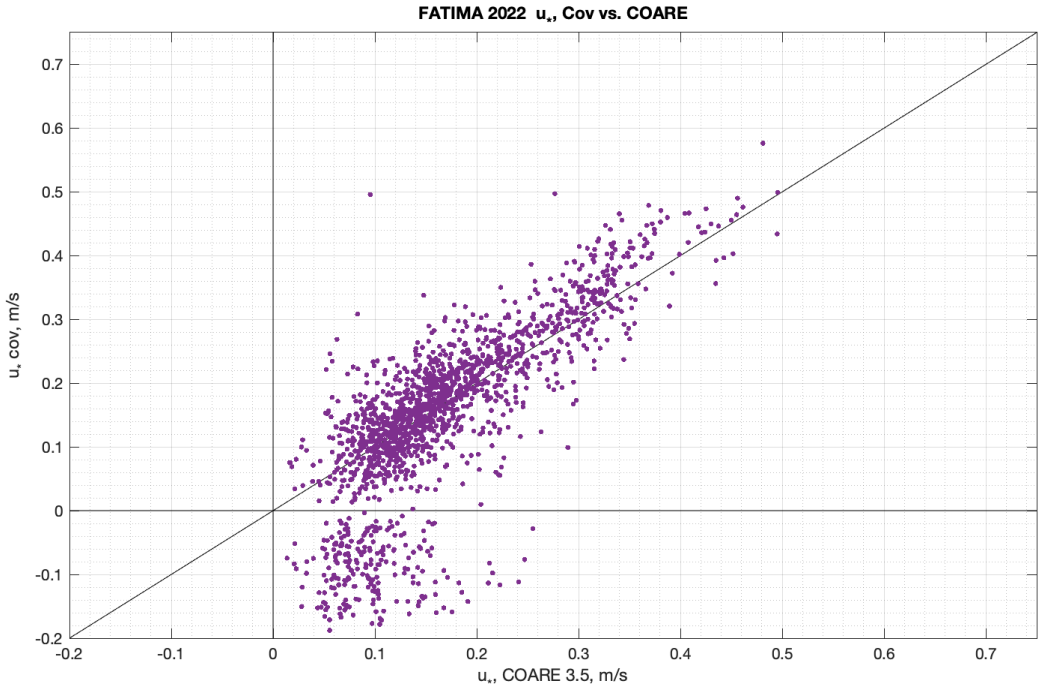

Figure 26: Filtered 10-minute covariance vs. bulk friction velocity. See Appendix 1 for specific filtering criteria.

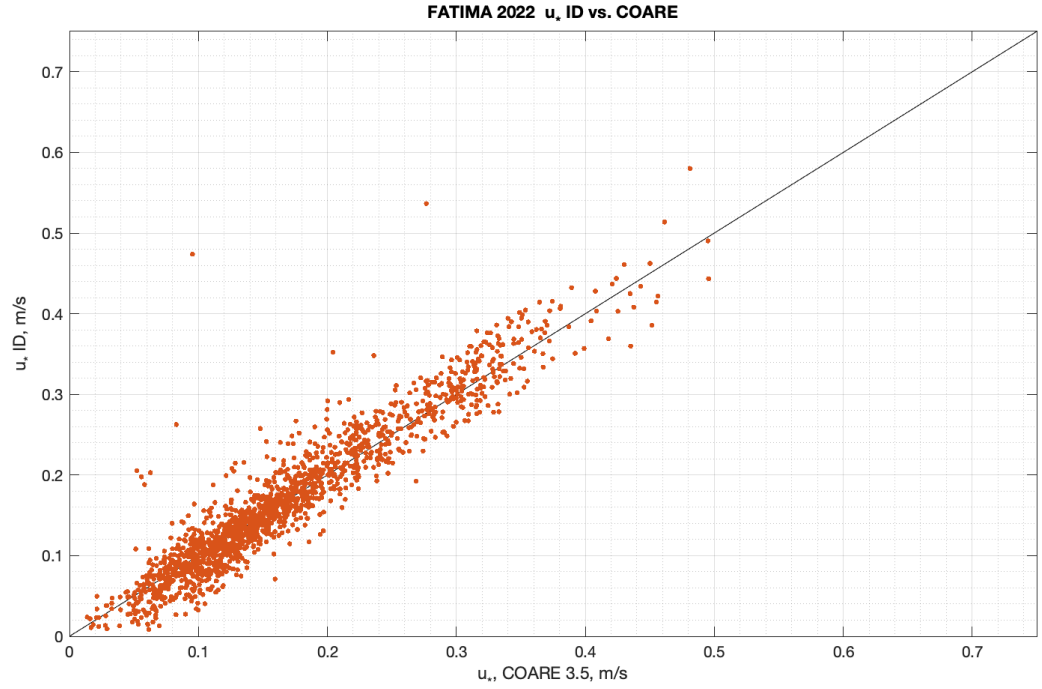

Figure 27: Filtered 10-minute inertial dissipation vs. bulk friction velocity.

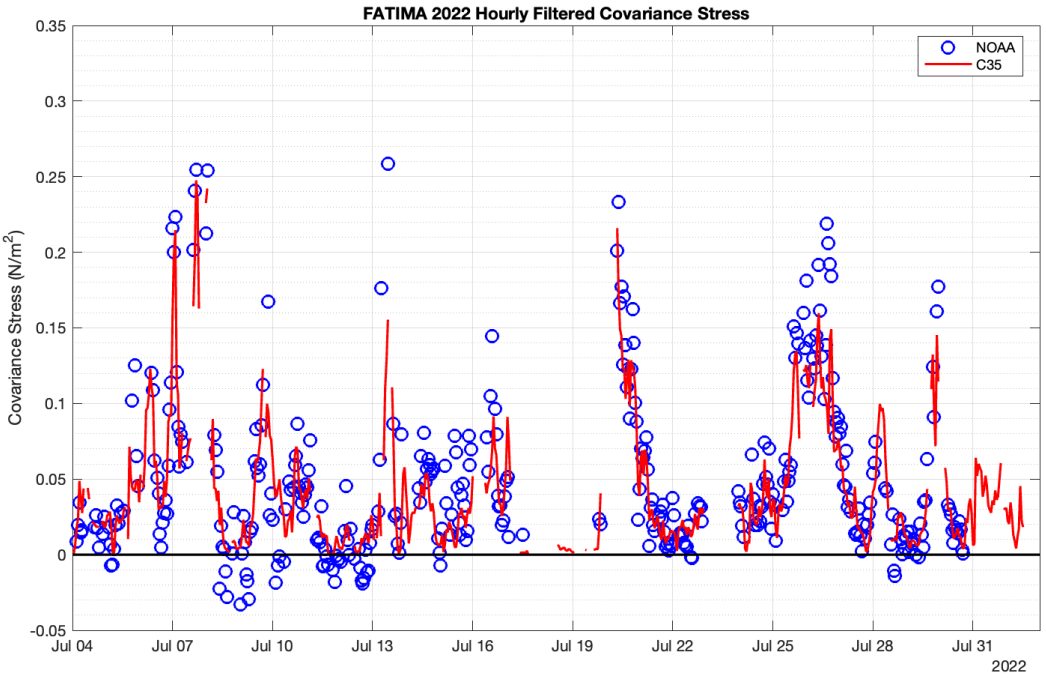

Figure 28: Hourly filtered covariance stress time series. Red line is the COARE 3.5 bulk estimate.

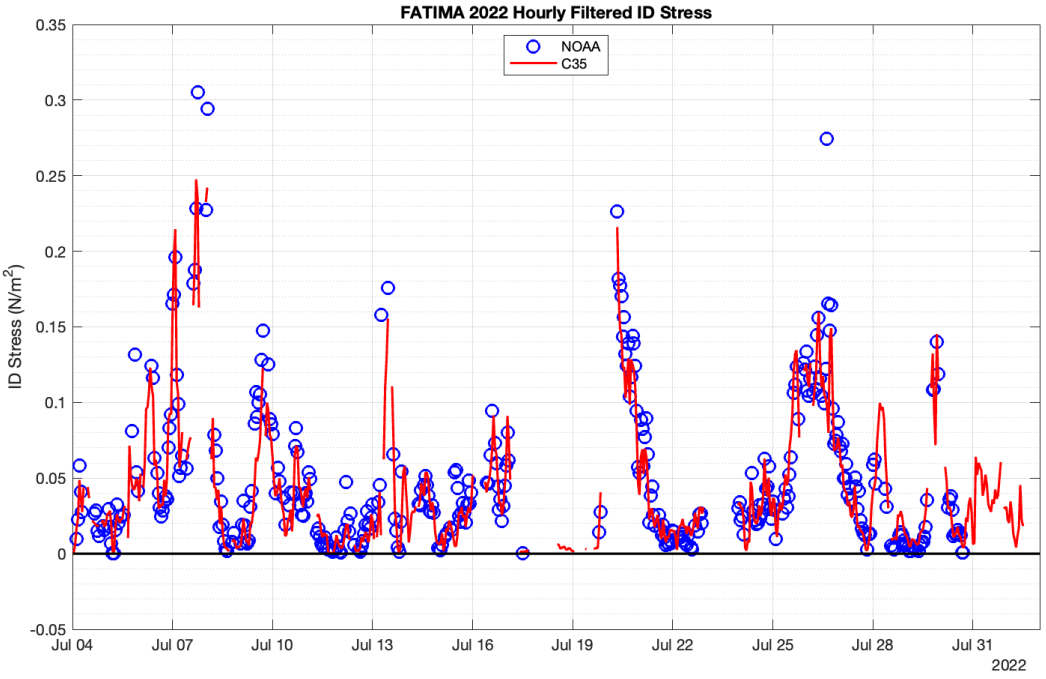

Figure 29: Hourly filtered inertial dissipation stress time series. Red line is the COARE 3.5 bulk estimate.

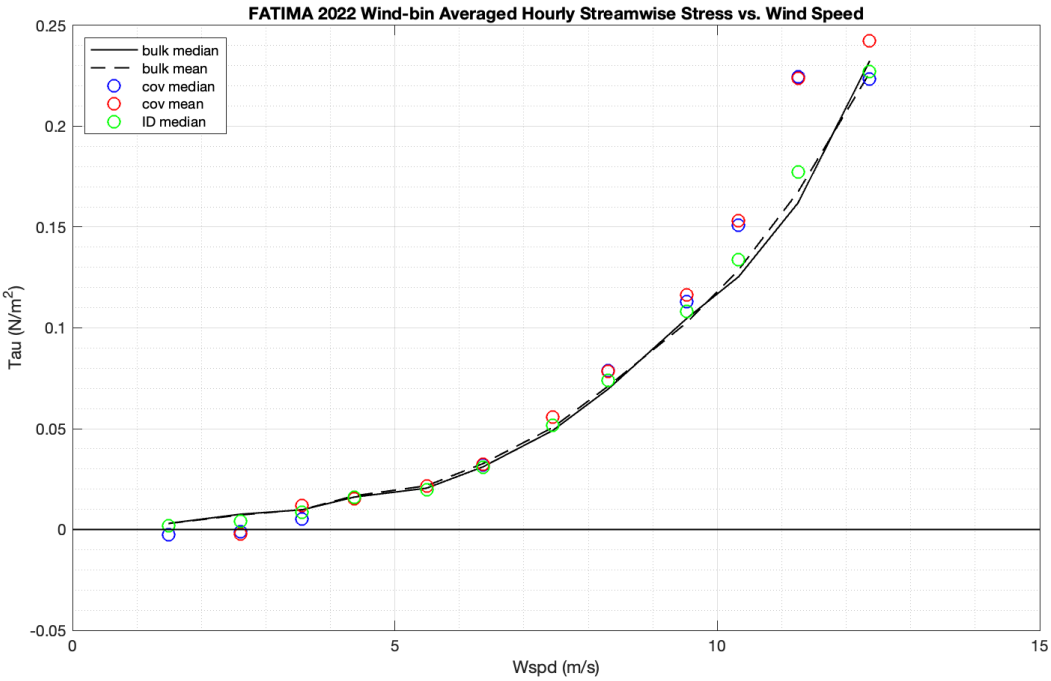

Figure 30: Stress vs. wind speed, covariance and bulk.

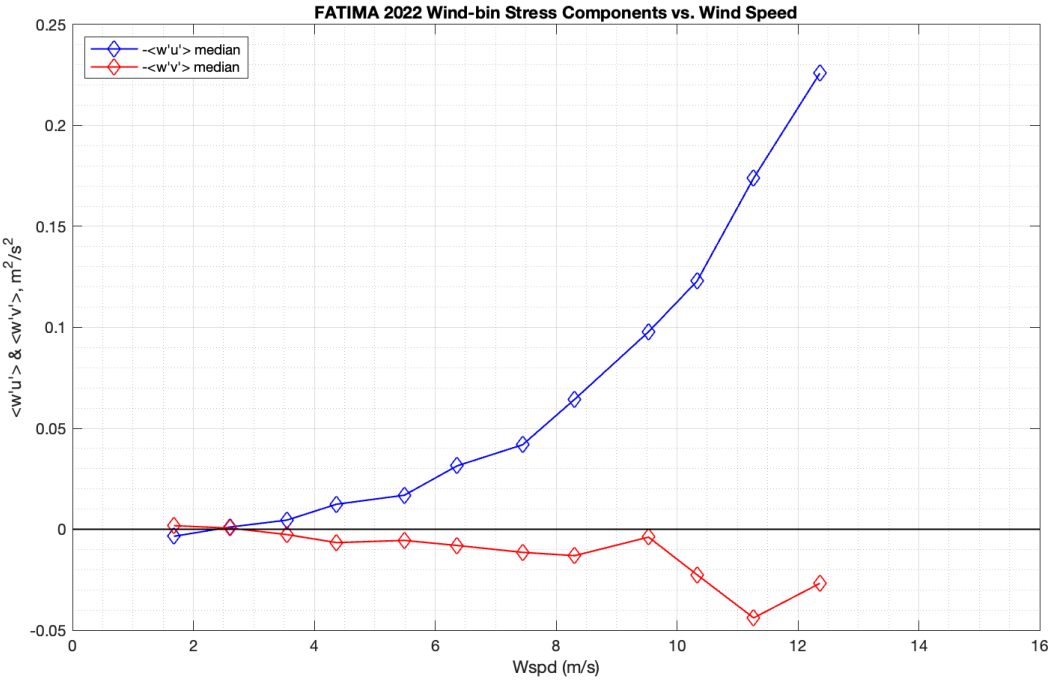

Figure 31: Streetwise and cross-stream covariance stress vs. wind speed.

Latent heat flux

Open-path infrared gas analyzers such as the Licor 7500 only operate reliably when the optics are clean and dry. As expected, this presents a challenge in the high-humidity, foggy conditions encountered during FATIMA. Figure 36 shows the time series of specific humidity and the Licor AGC quality control parameter. AGC values less than 60 indicate acceptable signal levels. This condition is met 38% of the time.

Licor specific humidity is biased high during Leg 1 due to incorrect calibration constants in the analyzer processor. This was fixed during the layover in St. John's by swapping the Licor head. When the equipment returns from the field we can recover the calibration constants from the analyzer electronics and reprocess the Leg 1 measurements.

Latent heat flux is computed from the cospectrum as

$$HL = L_e \, \rho_a \, |w'q'|$$

where L_e is latent heat of evaporation. A correction is applied for density fluctuations related to the heat fluxes (i.e the 'Webb' effect). This is computed by the COARE bulk model from the bulk mean vertical velocity as

$$HL_{webb} = L_e \, \rho_a \, q \, \overline{w}$$

Figure 37 shows the time series of filtered hourly latent heat flux ($HL + HL_{webb}$). Both covariance and ID HL show a slight positive bias compared to the bulk model of ~ 5 W/m^2 (Figures 38 & 39).

Comparison with bulk heat formulas

From the bulk formulas for temperature and humidity flux

$$\overline{w'T'} = U_{10n} \, C_{h10n} \, (T_{sfc} - \Theta_{10})$$

$$\overline{w'q'} = U_{10n} \, C_{e10n} \, (q_{sfc} - q_{10n})$$

We expect a plot of observed $\overline{w'T'}/U_{10n}$ vs. $(T_{sfc} - \Theta_{10})$ to pass through the origin with a slope equal to C_{h10n}, which is commonly taken to be ~ 1 x 10^{-3}. A similar plot can be constructed for the humidity flux relationship.

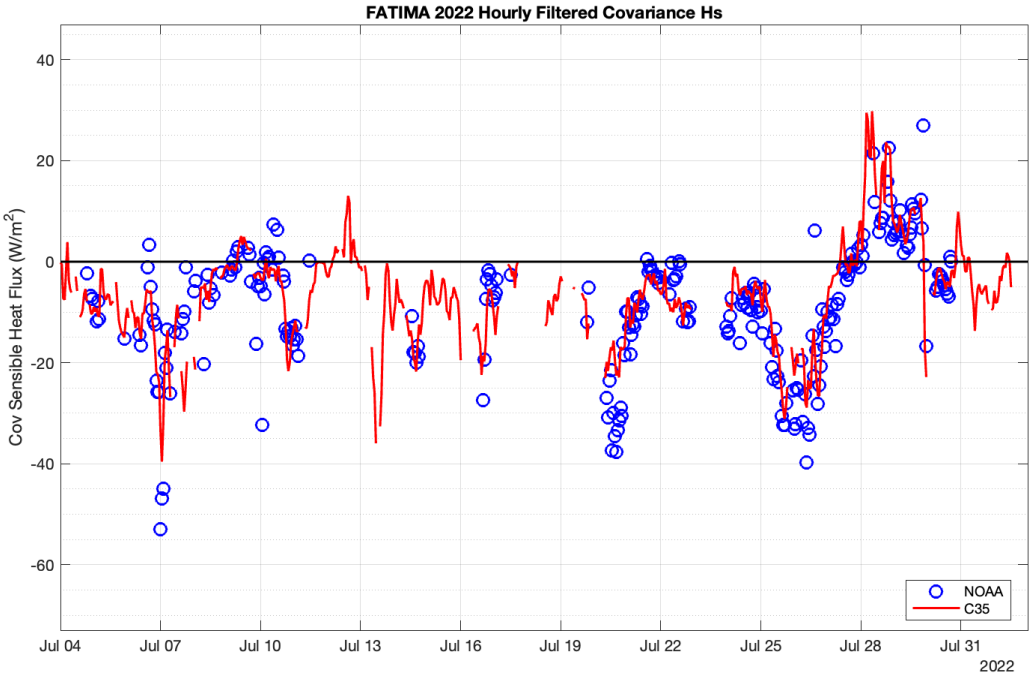

Figure 32: Hourly filtered covariance sensible heat flux.

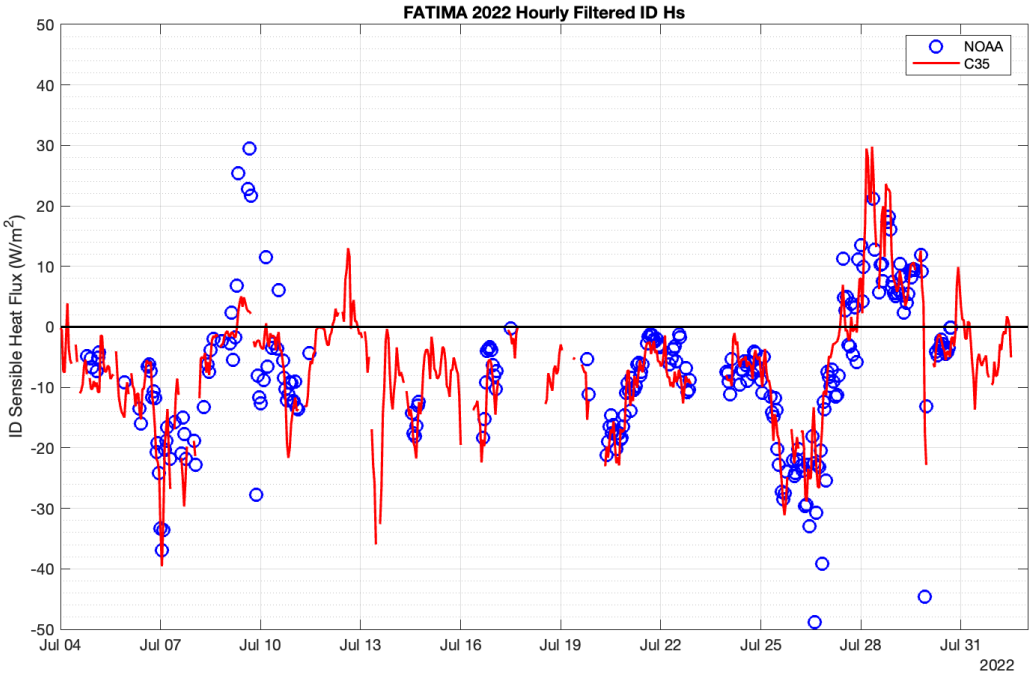

Figure 33: Hourly filtered inertial dissipation sensible heat flux.

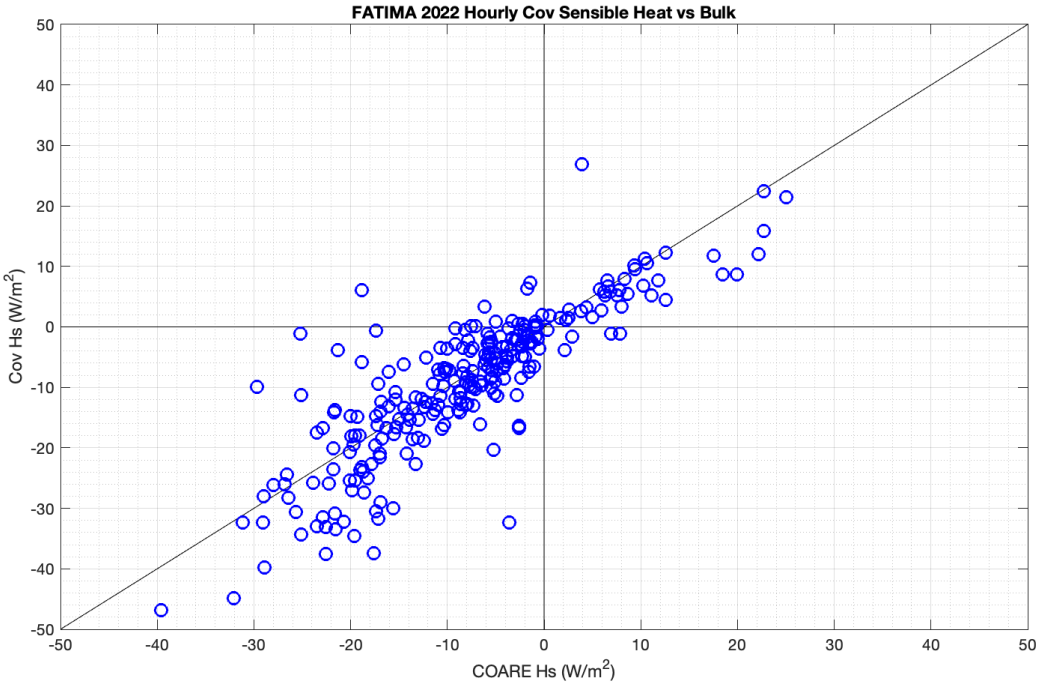

Figure 34: Hourly filtered covariance sensible heat flux vs. bulk.

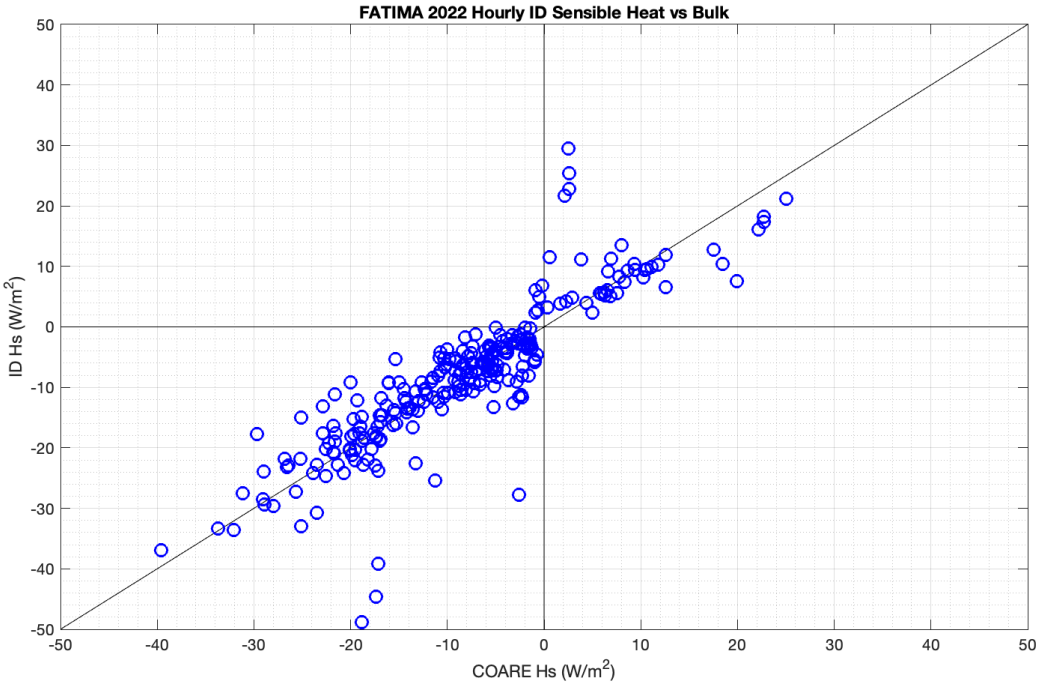

Figure 35: Hourly filtered inertial dissipation sensible heat flux vs. bulk.

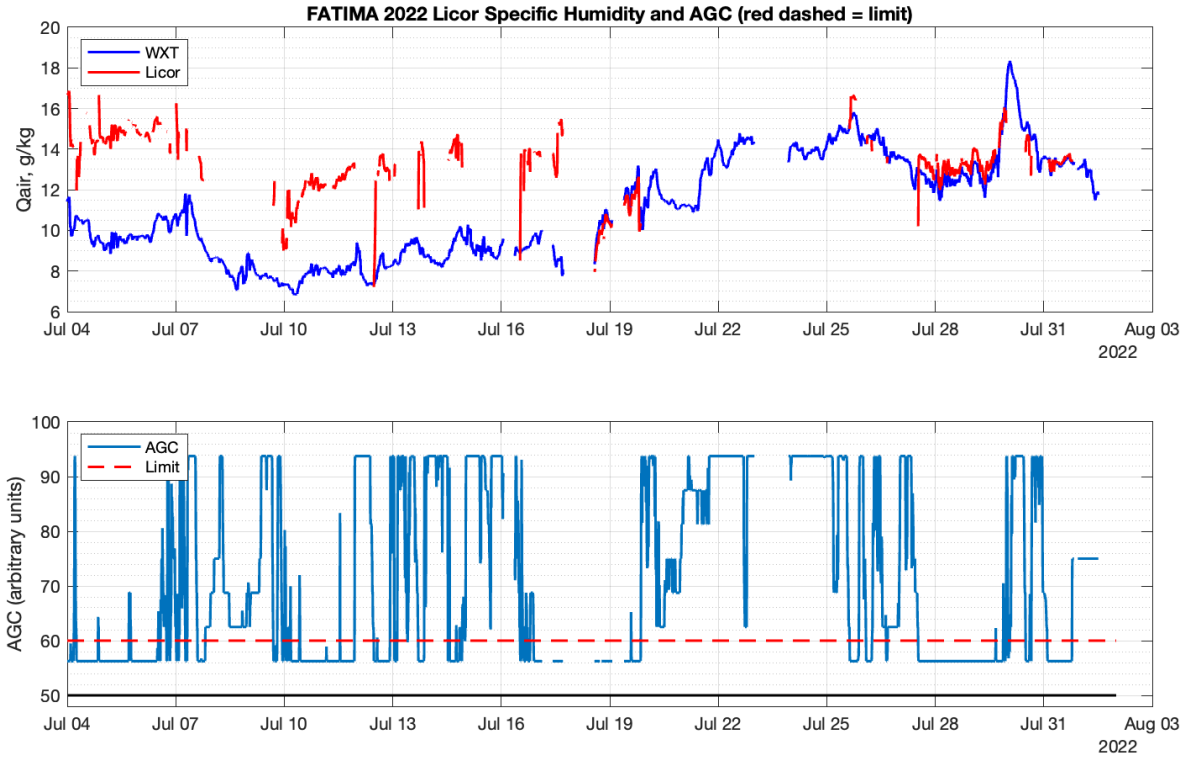

Figure 36: Specific humid and quality control (Auto Gain Control) for the Licor 7500 infrared gas analyzer. AGC < 60 (red dashed line) indicates 'good' data.

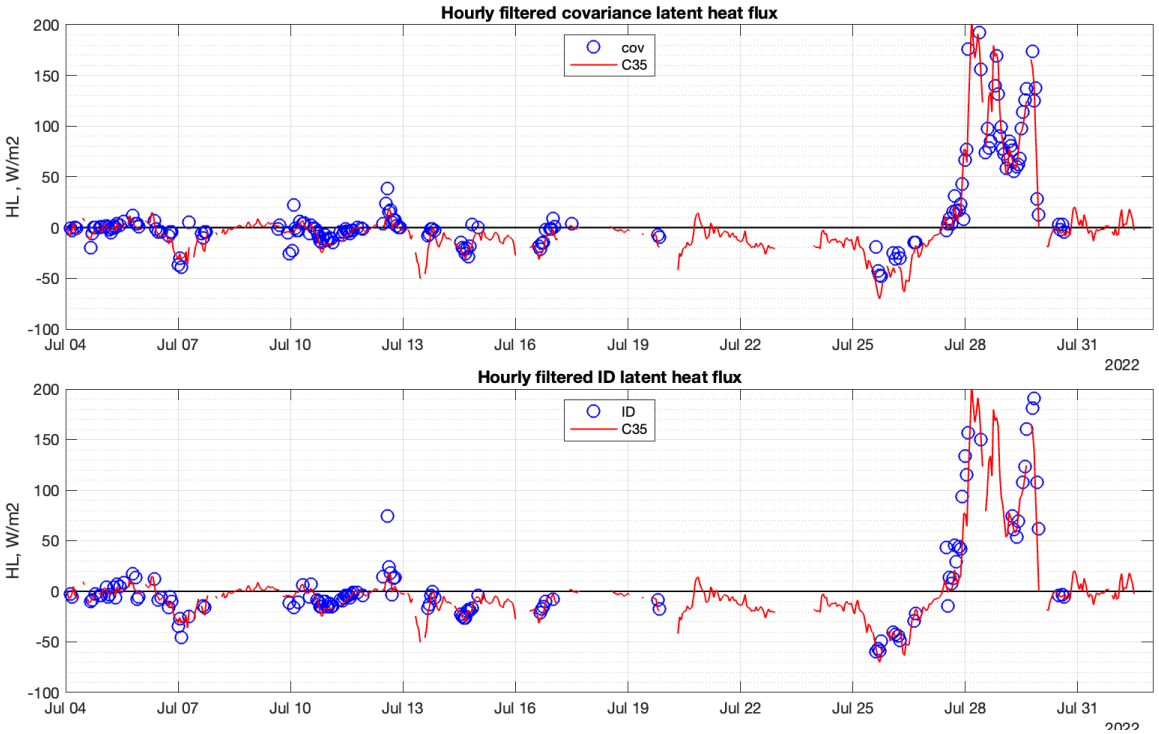

Figure 37: Hourly filtered covariance and ID latent heat flux (Webb corrected) from the Licor 7500.

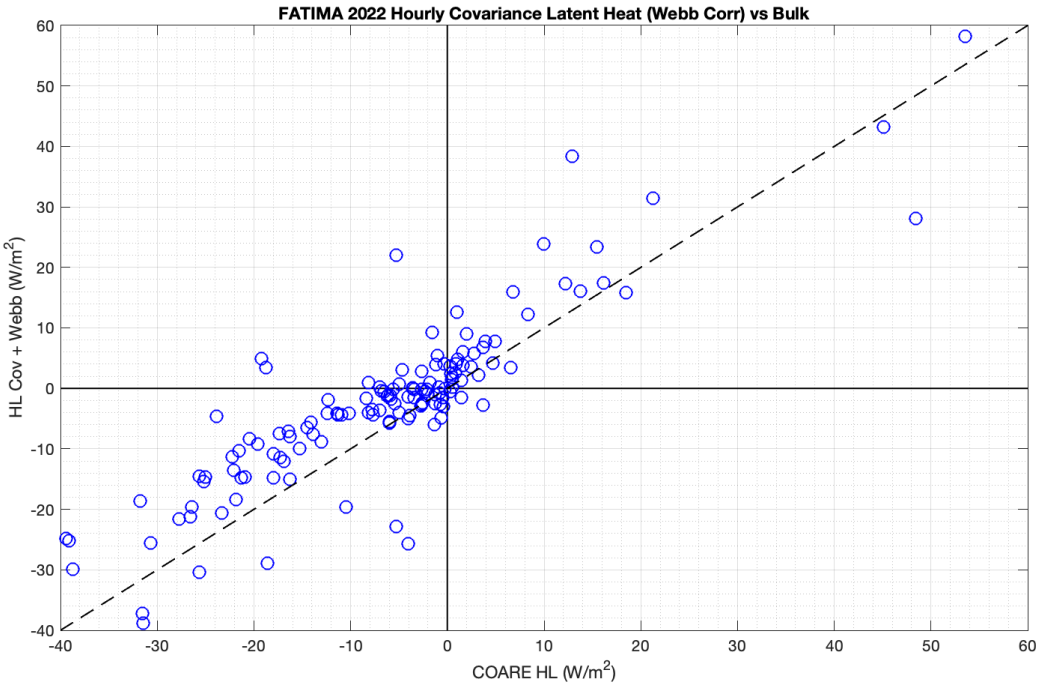

Figure 38: Filtered hourly covariance latent heat flux vs. bulk.

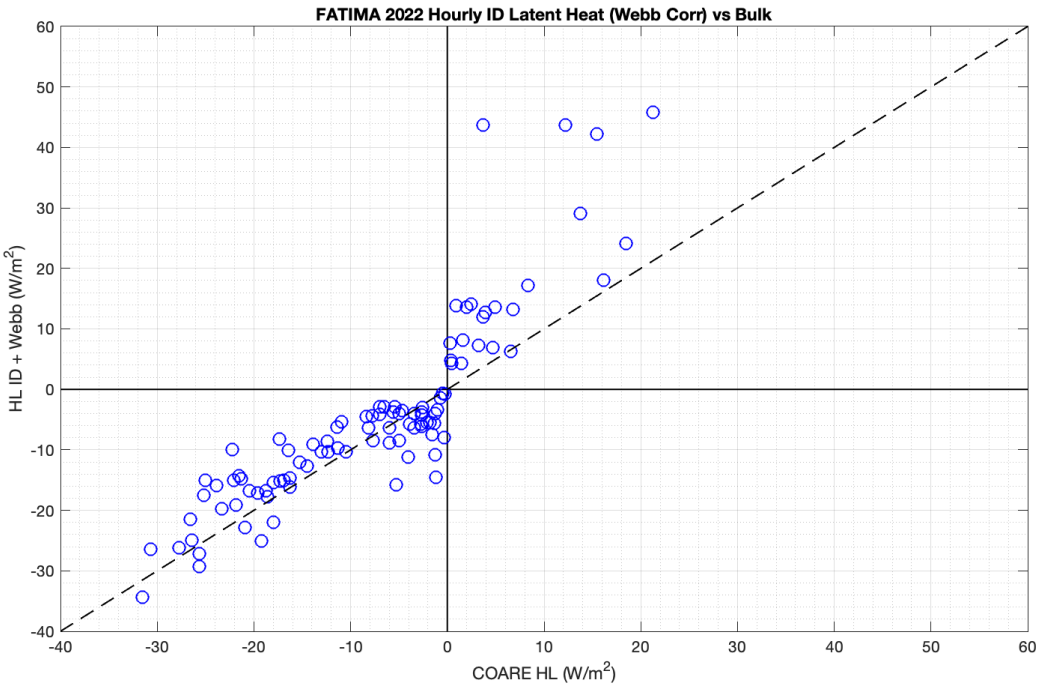

Figure 39: Filtered hourly ID latent heat flux vs. bulk.

The magnitude of the x-intercept can indicate the degree of potential bias in the ΔT and Δq terms. Figures 40 and 41 show that filtered 10-min results from FATIMA agree quite well with the expected result, especially for sensible heat flux.

Remaining issues

As mentioned above, a recalibration of Licor 7500 water vapor measurements should be done after equipment returns from the field. We don't expect the recalibration to have a large impact on the observed flux since it appears to be largely a bias adjustment.

The difference in nighttime temperature measurements from the WXT and PIR case dome sensors should also be examined when once gear is back in the lab. As mentioned above, flux results look better if we do not adjust the WXT measurement. The PIR temperatures may all be biased by ~ 0.5°C. Or, there may have been a consistent difference at the location of the radiometers that would explain a positive temperature bias of this magnitude, such as proximity to the ship engine exhaust and ventilation exhaust emissions.

Further analysis may also lead to updates in the ROSR sea surface temperature or observed rain rate.

A second version of this dataset may be released at a future date if necessary to resolve these issues.

References

Edson, J. B., Hinton, A. A., Prada, K. E., Hare, J. E., and Fairall, C. W., Direct covariance flux estimates from mobile platforms at sea, J. Atmos. Ocean. Tech., 15, 547–562, 1998.

Kaimal, J.C. and Finnigan, J.J., "Atmospheric Boundary Layer Flows, Their Structure and Measurement", Oxford Univ. Press, 1994.

Iqbal, M. in "Physical Climatology for Solar and Wind Energy", World Scientific, 1988, pp. 196-242.

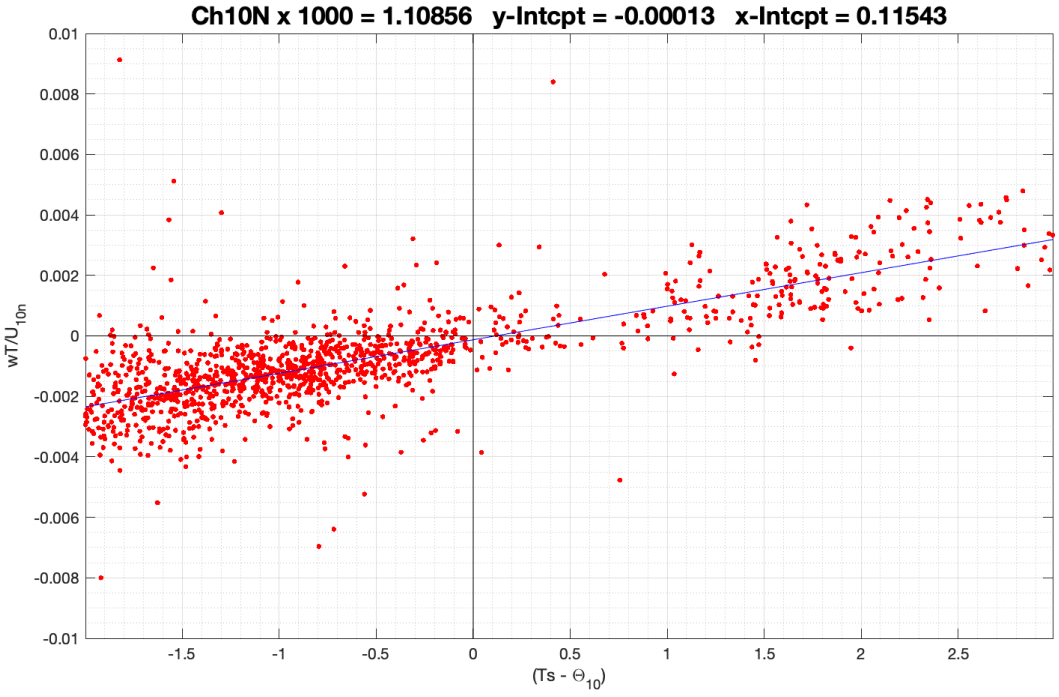

Figure 40: Analysis of observed temperature flux and gradient.

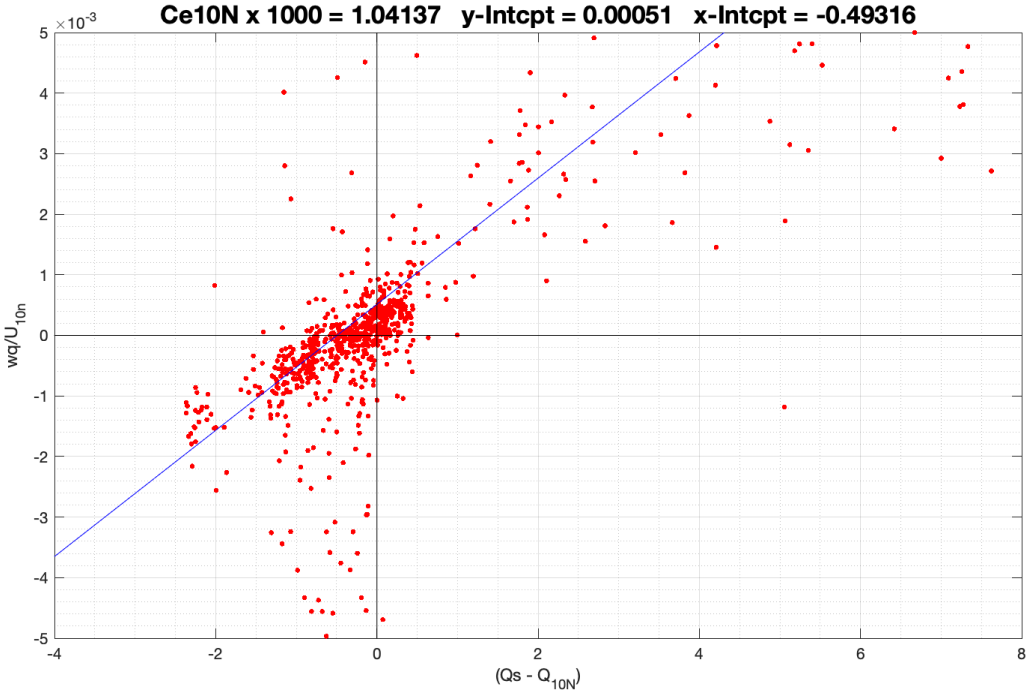

Figure 41: Analysis of observed water humidity flux and gradient.

Appendix 1: Data filters

Ten minute results

Raw 10-minute true wind measurements are filtered for relative wind direction with a sector for valid data of +/- 120°. Relative wind and tilt angle is not filtered. Sea snake SST is removed for all times after 17 July 0600 hours due to a problem with the sensor cabling. Other bulk meteorological and radiation measurements are not filtered.

Raw Licor water vapor variables and turbulence latent heat fluxes are filtered with criteria shown in Table 1 to remove outliers and periods with poor signal. Raw turbulence variables and fluxes are filtered with crude limits shown in Table 2.

Final 10-min output variables (see Appendix 2) are derived from the filtered raw 10-min product.

Hourly results

The filtered10-min turbulent flux results are further filtered according to additional criteria in Table 3 and averaged to hourly values for the final flux product.

Table 1: Licor filters for 10-min data

Variables	Filter metric	Limits for 'good' data
h2o, co2, wq, hl, Cq2	AGC	< 60
h2o, co2, wq, hl, Cq2	co2 concentration	200 ppm < co2 < 700 ppm
h2o, co2, wq, hl, Cq2	missing data points per 10 min segment	< 5% of total points expected in 10 min
wq	limit value of computed wq	-0.2 < wq < 0.2 g/kg m/s

Table 2: General filters for raw 10-min turbulence/flux data

Variables	Filter metric	Limits for 'good' data
wu, wv, wTs, wT, wq, hs, hl, Cu2, Cw2, Ct2, Cq2, usib, qsib, tsib, Lid	missing sonic wind, motion or heading data per 10 min segment	< 5% of total points expected in 10 min
wu, wv, wTs, wT, wq, hs, hl, Cu2, Cw2, Ct2, Cq2, usid, qsid, tsid, Lid	limit the number of bad (NaN) sonic wind data points per 10 min segment	badPnts < 100
wu	limit value of computed wu	-0.8 < wu < 0.1
wv	limit value of computed wv	-0.2 < wv < 0.2
wTs, wT	limit value of computed wT	-0.25 < wT < 0.25
Cu2	limit value of computed Cu2	0 < Cu2 < 1
Cw2	limit value of computed Cw2	0 < Cw2 < 1
Ct2	limit value of computed Ct2	1e-6 < Ct2 < 0.6
Cq2	limit value of computed Cq2	1e-4 < Cq2 < 0.2
wT, wTs, Ct2	limit Tsonic variance	σ^2 Tsonic < 0.15
wT, wTs, Ct2	limit Tsonic spectral noise	Ts_noise < 1e-3

Table 3: Additional filters for hourly means

Variables	Filter metric	Limits for 'good' data
cu, cw ct, cq, hs, hsib, hl, hlib, tauc, taucx, tauib	10 min relative wind direction	-90 < rwdir < 90
cu, cw ct, cq, hs, hsib, hl, hlib, tauc, taucx, tauib	10 min std dev heading	std_hed < 5°
cu, cw ct, cq, hs, hsib, hl, hlib, tauc, taucx, tauib	10 min std dev SOG	std_sog < 1.5 m/s
cu, cw ct, cq, hs, hsib, hl, hlib, tauc, taucx, tauib	10 min mean rain rate	rain < 1 mm/hr
cu, cw ct, cq, hs, hsib, hl, hlib, tauc, taucx, tauib	10 min std dev port-stbd velocity	vplat_std < 0.8 m/s
cu, cw, tauc, taucx, tauib	difference in cov and ID stress	abs(wu - usib^2) < 0.2 + 0.006*wspd

Appendix 2: Data file description

10-min Result File (matlab table and ascii text formats)

col	variable	units	description
1	dnum	none	matlab datenum timestamp (decimal day)
2	wspd	m/s	true wind speed
3	wdir	deg	true wind direction
4	rwspd	m/s	relative wind speed
5	rwdir	deg	relative wind direction
6	ta	°C	air temperature
7	ta_wxt	°C	air temperature, WXT sensor
8	rh	percent	relative humidity
9	rh_wxt	percent	relative humidity, WXT sensor
10	sst	°C	sea surface temperature
11	sst_rosr	°C	radiometruc sea surface temperature
12	Pmb	mb	sea level air pressure
13	qs	g/kg	surface saturation specific humidity
14	qa	g/kg	specific humidity
15	rs	W/m2	downwelling solar radiative flux
16	rl	W/m2	downwelling IR flux
17	rain	mm/hr	rain rate
18	hsc	W/m2	turbulent sensible heat flux
19	hsib	W/m2	inertial dissipation sensible heat flux
20	hsb	W/m2	bulk sensible heat flux
21	hlc	W/m2	turbulent latent heat flux
22	hlib	W/m2	inertial dissipation latent heat flux
23	hlb	W/m2	bulk latent heat flux
24	tauc	N/m2	turbulent streamwise wind stress
25	tauxc	N/m2	turbulent cross-stream wind stress
26	tauib	N/m2	inertial dissipation wind stress
27	taub	N/m2	bulk wind stress
28	ct	none	Ct structure func parameter
29	cq	none	Cq structure func parameter
30	cu	none	Cu structure func parameter
31	cw	none	Cw structure func parameter
32	jplume	none	exhaust plume filter flag
33	jmanuv	none	ship maneuver filter flag
34	tilt	deg	streamline tilt at location of sonic
35	RF	W/m2	rain heat flux
36	hlwebb	W/m2	latent heat 'Webb' correction

37	rlclr	W/m2	clear sky IR downwelling radiative flux
38	rsclr	W/m2	clear sky solar downwelling radiative flux
39	u10n	m/s	10m neutral wind speed
40	t10n	°C	10m neutral air temperature
41	q10n	g/kg	10m neutral specific humidity
42	usid_flag	none	quality flag for ID ustar
43	qsid_flag	none	quality flag for ID qstar
44	tsid_flag	none	quality flag for ID tstar
45	zu	m	wind measurement height
46	zt	m	air temperature measurement height
47	zq	m	humidity measurement height
48	hed	deg	ship heading
49	sog	m/s	ship speed over ground from gps
50	cog	deg	ship course over ground from gps
51	lat	degN	latitude
52	lon	degE	longitude
53	wspd_ship	m/s	true wind speed from ship sensor
54	wdir_ship	deg	true wind direction from ship sensor
55	ta_ship	°C	air temperature from ship sensor
56	rh_ship	percent	relative humidity from ship sensor
57	sst_ship	°C	sea surface temperature from ship sensor
58	Pmb_ship	mb	sea level air pressure from ship sensor
59	qs_ship	g/kg	surface sat. specific humidity from ship set
60	qa_ship	g/kg	specific humidity from ship sensor
61	rs_ship	W/m2	downwelling solar radiative flux, ship sensor
62	rl_ship	W/m2	downwelling IR flux, ship sensor
63	q_lic	g/kg	specific humidity from Licor 7500
64	q_lic_std	g/kg	std dev specific humidity from Licor 7500
65	co2_lic	ppm	co2 ppm from Licor 7500
66	co2_lic_std	ppm	std dev co2 ppm from Licor 7500

Hourly Result File (matlab table and ascii text formats)

col	variable	units	description
1	dnum	none	matlab datenum timestamp (decimal day)
2	wspd	m/s	true wind speed
3	wdir	deg	true wind direction
4	rwspd	m/s	relative wind speed
5	rwdir	deg	relative wind direction
6	ta	°C	air temperature
7	ta_wxt	°C	air temperature, WXT sensor
8	rh	percent	relative humidity
9	rh_wxt	percent	relative humidity, WXT sensor
10	sst	°C	sea surface temperature
11	sst_rosr	°C	radiometruc sea surface temperature
12	Pmb	mb	sea level air pressure
13	qs	g/kg	surface saturation specific humidity
14	qa	g/kg	specific humidity
15	rs	W/m2	downwelling solar radiative flux
16	rl	W/m2	downwelling IR flux
17	rain	mm/hr	rain rate
18	hsc	W/m2	turbulent sensible heat flux
19	hsib	W/m2	inertial dissipation sensible heat flux
20	hsb	W/m2	bulk sensible heat flux
21	hlc	W/m2	turbulent latent heat flux
22	hlib	W/m2	inertial dissipation latent heat flux
23	hlb	W/m2	bulk latent heat flux
24	tauc	N/m2	turbulent streamwise wind stress
25	taucx	N/m2	turbulent cross-stream wind stress
26	tauib	N/m2	inertial dissipation wind stress
27	taub	N/m2	bulk wind stress
28	ct	none	Ct structure func parameter
29	cq	none	Cq structure func parameter
30	cu	none	Cu structure func parameter
31	cw	none	Cw structure func parameter
32	jplume	none	exhaust plume filter flag
33	jmanuv	none	ship maneuver filter flag
34	tilt	deg	streamline tilt at location of sonic
35	RF	W/m2	rain heat flux
36	hlwebb	W/m2	latent heat 'Webb' correction
37	rlclr	W/m2	clear sky IR downwelling radiative flux
38	rsclr	W/m2	clear sky solar downwelling radiative flux
39	u10n	m/s	10m neutral wind speed

40	t10n	°C	10m neutral air temperature
41	q10n	g/kg	10m neutral specific humidity
42	usid_flag	none	quality flag for ID ustar
43	qsid_flag	none	quality flag for ID qstar
44	tsid_flag	none	quality flag for ID tstar
45	zu	m	wind measurement height
46	zt	m	air temperature measurement height
47	zq	m	humidity measurement height
48	hed	deg	ship heading
49	sog	m/s	ship speed over ground from gps
50	cog	deg	ship course over ground from gps
51	lat	degN	latitude
52	lon	degE	longitude
53	wspd_ship	m/s	true wind speed from ship sensor
54	wdir_ship	deg	true wind direction from ship sensor
55	ta_ship	°C	air temperature from ship sensor
56	rh_ship	percent	relative humidity from ship sensor
57	sst_ship	°C	sea surface temperature from ship sensor
58	Pmb_ship	mb	sea level air pressure from ship sensor
59	qs_ship	g/kg	surface sat. specific humidity from ship set
60	qa_ship	g/kg	specific humidity from ship sensor
61	rs_ship	W/m2	downwelling solar radiative flux, ship sensor
62	rl_ship	W/m2	downwelling IR flux, ship sensor
63	q_lic	g/kg	specific humidity from Licor 7500
64	q_lic_std	g/kg	std dev specific humidity from Licor 7500
65	co2_lic	ppm	co2 ppm from Licor 7500
66	co2_lic_std	ppm	std dev co2 ppm from Licor 7500
67	rnl	W/m2	net longwave radiation (into ocean)
68	hnetb	W/m2	net heat flux into ocean, bulk hs & hl
69	hnetc	W/m2	net heat flux into ocean, turb hs & hl
70	hnetib	W/m2	net heat flux into ocean, ID hs & hl

Archive directory structure

FATIMA_2022 - root directory

_matlab - data processing scripts and subroutines

_python - auxiliary data processing scripts

processed - final 10-min and hourly results in .mat and .txt formats. Subfolders of intermediate data files from `a2_motcorr_flux_FATIMA_2022.m`

da_decorr - 10-min bulk met and fluxes.

motion_decorr - hourly platform motion @ 10 Hz.

sp_decorr - daily files of 10-min spectra/cospectra.

uvwStream_decorr - hourly files of 10Hz motion corrected wind.

processed_images - variety of data plots

daily_decorr - daily data plots from `a2_motcorr_flux_FATIMA_2022.m`

final_plots_png - analysis plots from `a3_final_filtered_FATIMA_2022.m`

spectra_decorr - spectra/cospectra from `a2_motcorr_flux_FATIMA_2022.m`

wind_plots_decorr - diagnostic plots from motion correction process

raw - folders of raw hourly ascii text data files

raw_daily_merge - daily matlab tables of raw data @ 1Hz

raw_images - folders of daily QA/QC and time series plots of raw data.

report - this report

There are three Matlab data processing scripts:

`a1_process_daily_FATIMA_2022.m` : this script was used to monitor data quality in the field. It produces a variety of QA/QC and data time series plots and saves summary r1 Hz aw data in matlab tables. It is not necessary to run this script again unless you wish to regenerate the QA/QC plots or 1 Hz summary files. Output from this script is not used in the final data processing and analysis

`a2_motcorr_flux_FATIMA_2022.m`: this is the primary data processing script with computes motion corrections to the 10 Hz wind, 10-min mean bulk quantities, turbulent parameters, and fluxes. A variety of plots are produced and saved to the *daily_decorr* and *spectra_decorr* folders. Ten minute output is saved to 'da' tables in the *da_decorr* folder. These files are the raw input for the final data analysis. Rerun this script to make adjustments to the motion correction or flux computation algorithm. Note, the script runs much faster if plotting is turned off.

`a3_final_filtered_FATIMA_2022.m`: the final analysis script. Filters raw 10-min results and computes hourly mean fluxes. Produces a variety of analysis plots in the *final_plots_png* folder. Saves final results in 10-min and hourly files as matlab tables and ascii text in the *processed* folder.

Note, consult subroutines in the *_matlab/FATIMA_subs* folder for details on how the raw data files are read and pre-processed into matlab tables for use in the scripts above.